The Roles of β-Oxidation and Cofactor Homeostasis in Peroxisome Distribution and Function in *Arabidopsis thaliana*

Mauro A. Rinaldi,* Ashish B. Patel,*,[1] Jaeseok Park,*,[2] Koeun Lee,* Lucia C. Strader,[†] and Bonnie Bartel*,[3]
*Department of Biosciences, Rice University, Houston, Texas 77005 and [†]Department of Biology, Washington University in St. Louis, Missouri 63130
ORCID IDs: 0000-0001-7087-1184 (M.A.R.); 0000-0002-7600-7204 (L.C.S.); 0000-0002-6367-346X (B.B.)

ABSTRACT Key steps of essential metabolic pathways are housed in plant peroxisomes. We conducted a microscopy-based screen for anomalous distribution of peroxisomally targeted fluorescence in *Arabidopsis thaliana*. This screen uncovered 34 novel alleles in 15 genes affecting oil body mobilization, fatty acid β-oxidation, the glyoxylate cycle, peroxisome fission, and pexophagy. Partial loss-of-function of lipid-mobilization enzymes conferred peroxisomes clustered around retained oil bodies without other notable defects, suggesting that this microscopy-based approach was sensitive to minor perturbations, and that fatty acid β-oxidation rates in wild type are higher than required for normal growth. We recovered three mutants defective in PECTIN METHYLESTERASE31, revealing an unanticipated role in lipid mobilization for this cytosolic enzyme. Whereas mutations reducing fatty acid import had peroxisomes of wild-type size, mutations impairing fatty acid β-oxidation displayed enlarged peroxisomes, possibly caused by excess fatty acid β-oxidation intermediates in the peroxisome. Several fatty acid β-oxidation mutants also displayed defects in peroxisomal matrix protein import. Impairing fatty acid import reduced the large size of peroxisomes in a mutant defective in the PEROXISOMAL NAD^+ TRANSPORTER (PXN), supporting the hypothesis that fatty acid accumulation causes *pxn* peroxisome enlargement. The diverse mutants isolated in this screen will aid future investigations of the roles of β-oxidation and peroxisomal cofactor homeostasis in plant development.

KEYWORDS peroxisome; lipid mobilization; fatty acid β-oxidation; PXN; PME31

PEROXISOMES are dynamic single lipid bilayer-bound organelles present in most eukaryotes that compartmentalize crucial steps of many metabolic pathways (Gabaldon 2010). Plant peroxisomes house β-oxidation and key steps of photorespiration, nitrogen metabolism, and plant hormone biosynthesis (reviewed in Hu *et al.* 2012).

One conserved function of peroxisomes is fatty acid β-oxidation (Figure 1), which is exclusively peroxisomal in plants. Oilseed plants, including *Arabidopsis thaliana*, obtain energy for postgerminative development by β-oxidizing fats stored as triacylglycerol (TAG) in oil bodies (reviewed in Chapman *et al.* 2012). The lipase SUGAR-DEPENDENT1 (SDP1) hydrolyzes oil body TAG (Figure 1; Eastmond 2006). The resultant fatty acids are esterified with CoA to enter peroxisomes through PEROXISOMAL ABC TRANSPORTER1 (PXA1; Figure 1; Zolman *et al.* 2001b), also known as COMATOSE (Footitt *et al.* 2002) or PEROXISOME DEFECTIVE3 (Hayashi *et al.* 2002), which cleaves the CoA moiety upon transport (De Marcos Lousa *et al.* 2013). Inside peroxisomes, fatty acids are reactivated by LONG CHAIN ACYL-COA SYNTHETASE (LACS) 6 and 7, which add the CoA moiety necessary for entry into β-oxidation (Fulda *et al.* 2002). The four-step β-oxidation cycle starts with oxidation by one of five ACYL-COA OXIDASE (ACX) isozymes with overlapping specificities (Eastmond *et al.* 2000b; Adham *et al.* 2005). The next two steps are performed by the partially redundant MULTIFUNCTIONAL PROTEIN2 (MFP2) and ABNORMAL INFLORESCENCE MERISTEM1 (AIM1), which both have

doi: 10.1534/genetics.116.193169
Manuscript received June 30, 2016; accepted for publication September 6, 2016; published Early Online September 7, 2016.
Supplemental material is available online at www.genetics.org/lookup/suppl/doi:10.1534/genetics.116.193169/-/DC1.
[1]Present address: Feinberg School of Medicine, Northwestern University, Chicago, IL 60611.
[2]Present address: Department of Biology, Massachusetts Institute of Technology, Cambridge, MA 02139.
[3]Corresponding author: Department of Biosciences, Rice University, MS-140, 6100 Main St., Houston, TX 77005. E-mail: bartel@rice.edu

2-*trans*-enoyl-CoA hydratase and l-3-hydroxyacyl-CoA dehydrogenase activities (Richmond and Bleecker 1999; Rylott *et al.* 2006). Finally, a 3-ketoacyl-CoA thiolase such as PEROXISOME DEFECTIVE1 (PED1) releases acetyl-CoA and a shortened fatty acyl-CoA, which can undergo further rounds of β-oxidation (Figure 1; Hayashi *et al.* 1998; Germain *et al.* 2001). The glyoxylate cycle processes the liberated acetyl-CoA for the eventual production of sugars (reviewed in Graham 2008). ISOCITRATE LYASE (ICL) and MALATE SYNTHASE (MLS) catalyze peroxisomal steps of the glyoxylate cycle (Eastmond *et al.* 2000a; Cornah *et al.* 2004). Fatty acid β-oxidation defects ensue when the participating enzymes are dysfunctional, and also when valine catabolism is disrupted. β-HYDROXYISOBUTYRYL-COA HYDROLASE1 (CHY1) catalyzes a late step in valine catabolism (Figure 1; Zolman *et al.* 2001a). CHY1 impairment leads to accumulation of a toxic intermediate, methacrylyl-CoA, which inactivates the PED1 thiolase (Zolman *et al.* 2001a; Lange *et al.* 2004). Mutants with fatty acid β-oxidation defects inefficiently mobilize energy stores, resulting in growth defects that can be partially alleviated by providing an external carbon source such as sucrose (Hayashi *et al.* 1998; Zolman *et al.* 2000). These β-oxidation mutants also display additional defects that have not been completely explained (Rylott *et al.* 2003; Pinfield-Wells *et al.* 2005; Rylott *et al.* 2006; Footitt *et al.* 2007; Khan *et al.* 2012).

NAD^+ and CoA are key cofactors for β-oxidation (Figure 1). The peroxisomal membrane is permeable to small molecules up to 300–400 Da, but excludes bulkier cofactors such as ATP, NAD^+, and CoA (Antonenkov and Hiltunen 2012). PEROXISOMAL MALATE DEHYDROGENASE (PMDH) 1 and 2 recycle NADH to NAD^+ inside peroxisomes (Pracharoenwattana *et al.* 2007), and the glyoxylate cycle recycles CoA (reviewed in Graham 2008). *Arabidopsis* PEROXISOMAL NAD^+ CARRIER (PXN), also known as ABERRANT PEROXISOME MORPHOLOGY3 (Mano *et al.* 2011), transports NAD^+ (Bernhardt *et al.* 2012) and CoA (Agrimi *et al.* 2012) *in vitro*, and NAD^+ when expressed in yeast (van Roermund *et al.* 2016). Defects in PXN lead to minor lipid mobilization defects (Bernhardt *et al.* 2012) and enlarged peroxisomes (Mano *et al.* 2011). It is not understood why peroxisomes are enlarged when the PXN transporter is dysfunctional.

The auxin indole-3-acetic acid (IAA) is a vital plant hormone that regulates a plethora of developmental processes (reviewed in Woodward and Bartel 2005; Enders and Strader 2015). IAA can be obtained from the peroxisomal β-oxidation of the precursor indole-3-butyric acid (IBA; Figure 1; Strader and Bartel 2011). Similarly, a synthetic IBA analog, 2,4-dichlorophenoxybutyric acid (2,4-DB), is β-oxidized to the herbicide 2,4-dichlorophenoxyacetic acid (2,4-D; Wain and Wightman 1954; Hayashi *et al.* 1998). PXA1 is implicated in IBA transport into peroxisomes (Zolman *et al.* 2001b), and IBA-to-IAA conversion requires a set of β-oxidation enzymes that is partially distinct from those used in fatty acid β-oxidation (Zolman *et al.* 2007, 2008; Strader *et al.* 2011).

Peroxisomal matrix proteins are synthesized in the cytosol and imported post-translationally via a **p**eroxisome **t**argeting **s**ignal (PTS). The PTS1 is a C-terminal tripeptide (Gould *et al.* 1989), whereas PTS2 is a nonapeptide in the N-terminal region (Swinkels *et al.* 1991) that is removed inside the peroxisome (Helm *et al.* 2007). Mislocalization of peroxisomally targeted proteins to the cytosol can be observed when genes important for peroxisome formation are disabled (Mano *et al.* 2006; Ramón and Bartel 2010; Goto *et al.* 2011; Monroe-Augustus *et al.* 2011; Farmer *et al.* 2013; Burkhart *et al.* 2014; Goto-Yamada *et al.* 2014; Woodward *et al.* 2014). Mature peroxisomes can divide by fission, and defects in this process can lead to fewer peroxisomes, larger peroxisomes, clustered peroxisomes, increased peroxisomal prolongations called peroxules, or a combination of these phenotypes (Mano *et al.* 2004; Zhang and Hu 2008; Aung and Hu 2009; Fujimoto *et al.* 2009; Zhang and Hu, 2009, 2010).

To further our understanding of peroxisomal processes, we performed a microscopy-based forward-genetic screen for altered green fluorescent protein targeted to the peroxisome (GFP-PTS1) distribution in *Arabidopsis* seedlings. We identified 34 novel mutations in 15 genes involved in a variety of peroxisomal processes, including one gene, *PECTIN METHYLESTERASE31* (*PME31*), not previously implicated in peroxisome function. Most of the mutants displayed clustered peroxisomes around retained oil bodies and disrupted proteins involved in fatty acid utilization. Analyses of these mutants contributed to the understanding of cofactor balance inside peroxisomes and uncovered unexpected peroxisomal defects, such as peroxisomal matrix protein import defects, in several fatty acid β-oxidation mutants.

Materials and Methods

Plant materials

Wild type and mutants were in the Columbia-0 (Col-0) accession. The line expressing GFP-PTS1 driven by the constitutive cauliflower mosaic virus 35S promoter (*35S:GFP-PTS1*) was described previously (Zolman and Bartel 2004). Some reference mutants were from the *Arabidopsis* Biological Resource Center (ABRC) at Ohio State University: *drp3a-3* (SALK_066958), *mdar4-4* (SALK_068667), *mls-3* (SALK_002289), and *pxn-3* (SAIL_636F12). Other reference mutants were described previously: *acx1-2* (SALK_041464; Adham *et al.* 2005), *acx2-1* (SALK_006486; Adham *et al.* 2005), *acx1-2 acx2-1* (Adham *et al.* 2005), *chy1-1* (Zolman *et al.* 2001a), *icl-1* (Eastmond *et al.* 2000a), *lon2-2* (SALK_043857; Lingard and Bartel 2009), *pmdh1-1* (Pracharoenwattana *et al.* 2007), *pmdh1-1 pmdh2-1* (Pracharoenwattana *et al.* 2007), *pxa1-1* (Zolman *et al.* 2001b), *ped1-96* (Lingard and Bartel 2009), *pex14-1* (Monroe-Augustus *et al.* 2011), and *lon2-2*, *atg7-3*, and *lon2-2 atg7-6* expressing *35S:PTS2-GFP* (Farmer *et al.* 2013). We crossed our *35S:GFP-PTS1* line to *pxa1-1* and *ped1-96*, and obtained *pxa1-1 35S:GFP-PTS1* and *ped1-96 35S:GFP-PTS1*, respectively, by following the construct

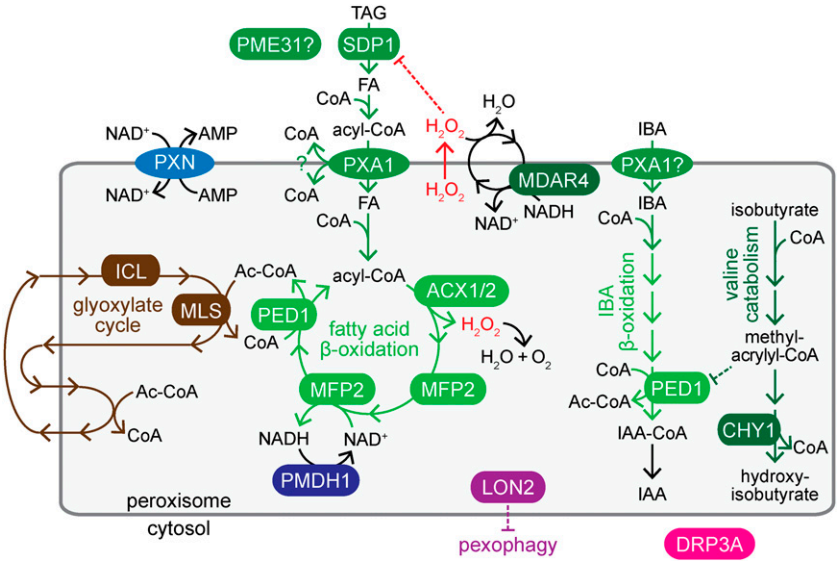

Figure 1 Peroxisomes house steps of key metabolic pathways; enzymes and transporters disrupted in mutants identified in this work are shown. Conversion of oil body triacylglycerol (TAG) to fatty acids (FA) requires SDP1. Fatty acids are activated with CoA in the cytosol and imported into peroxisomes by PXA1, which hydrolyzes the CoA upon transport. In the peroxisome, fatty acids are reactivated and catabolized to acetyl-CoA through β-oxidation (green), which requires ACX1/2, MFP2, and PED1 enzymes. ACX enzymes generate H_2O_2, which is detoxified by catalase (not shown), or by an MDAR4-dependent ascorbate peroxidase that inactivates H_2O_2 escaping from the peroxisome. CHY1 acts in valine catabolism downstream of methacrylyl-CoA, which can inactivate PED1. PME31 might aid in lipid mobilization. PXA1 is also implicated in peroxisomal import of IBA, and IBA-to-IAA β-oxidation likely involves dedicated enzymes (not shown) and PED1, which also acts in fatty acid β-oxidation. Carbon from β-oxidation-derived acetyl-CoA is converted to forms that can be shuttled out of the peroxisome via the glyoxylate cycle (brown), which includes ICL and MLS enzymes. PXN imports NAD^+, which is recycled by PMDH1/2; CoA is recycled in the glyoxylate cycle. LON2 is an ATP-dependent protease that restrains pexophagy. DRP3A is a peroxisome division factor.

and mutation in progeny by using fluorescence and PCR-based genotyping (Supplemental Material, Table S1).

For newly identified mutants, assays were conducted with twice-backcrossed lines (*pxn-4* and *mfp2-6*), once-backcrossed lines (*sdp1-7*, *mdar4-5*, *mdar4-6*/R541, *mdar4-7*, *pmdh1-2*, *acx1-4*, *acx2-3*, *mfp2-7*, *mfp2-8*, *mfp2-9*, *chy1-5*, *chy1-6*, *mls-4*, *lon2-8*, *lon2-10*, *pxn-4*, *drp3a-4*, *drp3a-5*, and *pme31-1*), or progeny from the original mutants (*mdar4-6*/R577, *pxa1-4*, *acx2-2*, *ped1-4*, *ped1-5*, *chy1-7*, *icl-3*, *icl-4*, *icl-5*, *pxn-4 lon2-8*, *lon2-9*, *pxn-5*, *pxn-6*, *pxn-7*, and *pme31-3*). For *pme31-2*, a backcrossed line that did not harbor the background mutations in *ACX2* and *IBA RESPONSE3* found through whole-genome sequencing was used for assays.

Growth conditions and phenotypic assays

Unless otherwise noted, surface-sterilized seeds were stratified and plated on plant nutrient medium (Haughn and Somerville 1986) solidified with 0.6% (w/v) agar and supplemented with 0.5% (w/v) sucrose in plates sealed with gas-permeable tape in growth chambers at 22° under continuous white fluorescent light. When treating with hormones dissolved in ethanol, control medium was normalized to the same ethanol content, and light was filtered through yellow long-pass filters to slow indolic compound breakdown (Stasinopoulos and Hangarter 1990). For hypocotyl elongation assays, plates were incubated under light for 1 day and then subjected to darkness by covering with two layers of aluminum foil. Root measurements of light-grown seedlings were performed at 8 days, and hypocotyl measurements of dark-grown seedlings were performed at 5 days. To assess lateral root production, seeds were sown on media and incubated for 4 days, then transferred to either media supplemented with hormones or media with no hormone for an additional 4 days. The number of lateral roots that protruded from the root epidermis was counted, root length was measured, and a ratio of these values was calculated.

Mutant isolation and identification

Wild-type (Col-0) *35S:GFP-PTS1* seeds were mutagenized with 0.24% ethyl methanesulfonate (EMS; Normanly 1997) for 16 hr. For screening, ~5000 M_2 seeds from each pool of 625 M_1 plants were placed in ~12 rows on five or six 100 × 100 mm square plates, and the plates were incubated horizontally for 1 day under constant white light before standing the plates nearly vertically. After 5 days, seedlings on plates were examined using a dissecting microscope equipped for GFP detection. We screened hypocotyls of ~160,000 M_2 seedlings from 32 M_1 pools for fluorescence distribution patterns that differed from wild-type puncta. Putative mutants were numbered, and given the prefix "*R*." Putative mutants were moved to soil, and 680 of 1020 produced progeny. We assayed for peroxisomal defects on the M_3 and M_4 progeny of these isolates by retesting GFP-PTS1 distribution using the dissecting microscope and testing for sucrose-dependent growth and IBA and 2,4-DB resistance. Promising lines were further tested for PTS2 processing using immunoblotting and for GFP-PTS1 localization using confocal microscopy.

Several mutants were backcrossed to Col-0 or Col-0 carrying GFP-PTS1 and/or outcrossed to the *A. thaliana* Landsberg *erecta* (*Ler*) accession. F_2 individuals from segregating populations were selected for either abnormal fluorescence or the strongest peroxisomal phenotype observed during the secondary screen (*e.g.*, IBA resistance and sucrose dependence). F_3 progeny from F_2 individuals displaying the phenotype of interest were tested for homogeneity of the selection phenotype as a proxy for homozygosity of the causal mutation.

Analyzing fluorescence in outcrossed populations revealed that the construct in our *35S:GFP-PTS1* line (Zolman and Bartel 2004) was located at the top of chromosome 5, likely between genes *At5g13000* and *At5g19000*. Causal mutations located in this region were identified through whole-genome sequencing (Thole and Strader 2015).

DNA analysis

DNA was prepared for PCR analysis as described (Celenza *et al.* 1995). For recombination mapping, progeny from mutant outcrosses to L*er* were genotyped using PCR-based markers that exploit polymorphisms to differentiate between Col-0 and L*er* DNA (Table S2). Overlapping PCR amplicons covering candidate genes of interest (Table S3) were sequenced by Lone Star Labs (Houston, TX). Nucleotide positions are reported relative to the first nucleotide in the first codon of the annotated gene.

Genomic DNA for whole-genome sequencing was prepared as previously described (Thole *et al.* 2014). DNA was sequenced with Illumina HiSequation 2000 sequencers by the Genome Technology Access Center at Washington University in St. Louis. Sequences were aligned with the *Arabidopsis* Col-0 genome from The Arabidopsis Information Resource (TAIR build 10) using Novoalign (Novocraft; http://novocraft.com), and mutations were identified using SAMtools (Li *et al.* 2009) and snpEFF (Cingolani *et al.* 2012). Mutations were filtered to obtain homozygous G-to-A or C-to-T transitions produced by EMS that resulted in nonsynonymous amino acid changes or altered splice sites in coding regions that are absent in our lab Col-0 line as described (Farmer *et al.* 2013).

Immunoblotting

Frozen tissue was homogenized in two volumes of 2× NuPAGE sample buffer (Invitrogen, Carlsbad, CA) and centrifuged at 16,100 × *g* for 5 min. Supernatants were heated at 100° for 5 min with 50 mM dithiothreitol. Samples were electrophoresed alongside prestained protein markers (P7708; New England Biolabs, Beverly, MA) and Cruz molecular mass markers (sc-2035; Santa Cruz Biotechnology, Santa Cruz, CA) on NuPAGE or Bolt 10% Bis-Tris gels (Invitrogen) using 1× MOPS running buffer [50 mM 3-(*N*-morpholino)-propanesulfonic acid, 50 mM Tris base, 0.1% sodium dodecyl sulfate, 1 mM EDTA] and transferred to Hybond Nitrocellulose membrane (Amersham Pharmacia Biotech) using NuPAGE transfer buffer (Invitrogen). Membranes were incubated for 1 hr at 4° in blocking solution (8% nonfat dry milk, 20 mM Tris pH 7.5, 150 mM NaCl, 0.1% Tween 20) and then incubated overnight at 4° with rabbit antibodies against PMDH2 (1:2000; Pracharoenwattana *et al.* 2007), thiolase (1:5000; Lingard *et al.* 2009), ICL (1:1000; Maeshima *et al.* 1988), or MLS (1:10,000; Olsen *et al.* 1993), or mouse antibodies against HSC70 (1:50,000; Stressgen SPA-817), diluted as indicated in blocking solution with 0.1% sodium azide. Membranes were incubated for 4 hr with secondary horseradish peroxidase-linked goat antibodies against rabbit or mouse IgG (1:5000; Santa Cruz Biotechnology; sc-2030 and sc-2031, respectively) diluted in blocking solution. Horseradish peroxidase was visualized using WesternBright ECL (Advansta) and exposing to autoradiography film. Films were imaged using a scanner. Membranes were incubated sequentially with different primary antibodies without stripping.

Microscopy

A Leica ZM10 F dissecting microscope equipped with filters for GFP detection was used to screen and retest hypocotyl GFP-PTS1 patterns at low (80×) magnification in 5-day-old light-grown seedlings.

For confocal microscopy, cotyledons from light-grown seedlings were excised and mounted in water. For Nile red staining, cotyledons were submerged in 5 μg/ml Nile red for at least 5 min. A Carl Zeiss LSM 710 laser scanning confocal microscope equipped with a 63× oil immersion objective and a Meta detector was used to image fluorescence. Tissue was excited with a 488-nm argon laser, and emission was collected between 493 and 526 nm for GFP, between 587 and 643 nm for Nile red, and between 688 and 757 nm for chlorophyll. Each image is an average of four exposures using a 24-μm pinhole, corresponding to a 1-μm optical slice. Epidermal cells were sometimes imaged at two points: midcell, where cytosolic fluorescence outlines the cell, and beneath the plasma membrane (subcortical), where cytosolic fluorescence has a diffuse pattern.

To estimate peroxisome size, fluorescent puncta in the GFP channel with cross-sectional areas > 1 μm^2 were measured using the "Analyze Particles" tool of ImageJ (http://imagej.nih.gov/ij/) from three 135 × 135 μm images. For each time point, all puncta detected in three images were plotted for the line (wild type or *pxn*) with the smaller number of puncta detected, and the same number of puncta (from one to three images; gathered by position in the image rather than size) were plotted for the other sample.

Data and reagent availability

Strains are available upon request. Sequence data can be found in the *Arabidopsis* Genome Initiative or GenBank/European Molecular Biology Laboratory databases using accession numbers in Table 1 and Table S4. Table S1 lists PCR-based markers used to genotype mutants and constructs. Table S2 lists PCR-based markers used for recombination mapping. Table S3 lists primers used to amplify and sequence candidate genes. Table S4 lists accession numbers of proteins used for alignments. Table S5 lists whole-genome sequencing strategies and results. Table S6 lists PCR-based genotyping markers used for recombination mapping in the backcross for R79 (*pme31-1*) and R363 (*pme31-2*). Table S7 summarizes the key phenotypes of the identified mutants. File S1 lists mutations identified through whole-genome sequencing.

Results

GFP-PTS1 localizes to distinct puncta in wild-type plant cells (Figure 2). To obtain new mutations in genes important for

Table 1 Mutants identified in a screen for altered peroxisomally-targeted fluorescence

Gene (accession number)	Function of protein	Allele	Alias	Nucleotide change	Protein or transcript change	Phenotypes *vs.* reference allele
Fatty acid β-oxidation						
SDP1 (*At5g04040*)	Triacylglycerol lipase	*sdp1-7*	R330	c1075t	Conserved R359W	Weaker[a]
PXA1 (*At4g39850*)	ATP binding cassette transporter	*pxa1-4*	R751	g1585a	G307E in EAA-like motif	Similar
ACX1 (*At4g16760*)	Acyl-CoA oxidase	*acx1-4*	R574	g1146a	Conserved G226R	Similar
ACX2 (*At5g65110*)	Acyl-CoA oxidase	*acx2-2*	R233	g603a	W154stop	Similar
		acx2-3	R737	g604a	Conserved G155R	Similar
MFP2 (*At3g06860*)	2-*trans*-Enoyl-CoA hydratase and l-3-hydroxyacyl-CoA dehydrogenase	*mfp2-6*	R281	g3737a	Conserved G670R	Similar[a]
		mfp2-7	R778	g2736a	Conserved A454T	Weaker[a]
		mfp2-8	R794/809	g2051a	Conserved G320D	Similar[a]
		mfp2-9	R1009	g2116a	Conserved E342K	Similar[a]
PED1 (*At2g33150*)	3-Ketoacyl-CoA thiolase	*ped1-4*	R814	g928a	Conserved G109E	Weaker
		ped1-5	R883	g1113a	Conserved G141E	Similar
Indirect fatty acid β-oxidation and glyoxylate cycle						
MLS (*At5g03860*)	Malate synthase (glyoxylate cycle)	*mls-4*	R332	g1595a	Intron 3 splice acceptor	Similar
ICL (*At3g21720*)	Isocitrate lyase (glyoxylate cycle)	*icl-3*	R291	g177a	Conserved E21K	Weaker
		icl-4	R601	g366a	Conserved G84R	Weaker
		icl-5	R951	g2128a	W371stop	Similar
PMDH1 (*At2g22780*)	Peroxisomal malate dehydrogenase (fatty acid β-oxidation)	*pmdh1-2*	R92	c643t	Q129stop	Similar
CHY1 (*At5g65940*)	β-Hydroxyisobutyryl-CoA hydrolase (valine catabolism)	*chy1-5*	R189	g700a	Conserved G119D	Similar
		chy1-6	R499/506	g871a	Conserved D150N	Similar
		chy1-7	R728	g988a	Conserved G165E	Similar
MDAR4 (*At3g27820*)	Peroxisomal monodehydroascorbate reductase (hydrogen peroxide detoxification)	*mdar4-5*	R340/343	g942a	Conserved G122D	Similar
		mdar4-6	R541/577	g31a	Conserved G11R	Similar
		mdar4-7	R923	g659a	Intron 2 splice acceptor	Similar
Large GFP-PTS1 puncta						
LON2 (*At5g47040*)	Peroxisomal protease	*lon2-8*	R109	g650a	Q102stop	Similar
		lon2-9	R498	g3610a	Conserved R537K in arginine finger of AAA+ domain	Weaker
		lon2-10	R973	g400a	W45stop	Similar
PXN (*At2g39970*)	Peroxisomal NAD+ and CoA transporter	*pxn-4*	R109	g2194a	Intron 9 splice acceptor	Similar
		pxn-5	R162	c2060t	R258stop	Similar
		pxn-6	R986	g1629a	Intron 6 splice acceptor	Similar
		pxn-7	R987/995	g2111a	Conserved G275E	Similar
Miscellanea						
DRP3A (*At4g33650*)	Dynamin-related protein (peroxisome division)	*drp3a-4*	R224	c755t	Q224stop	Similar
		drp3a-5	R402	g281a	Conserved R94H	Similar
PME31 (*At3g29090*)	Pectin methylesterase	*pme31-1*	R79	g701c	Conserved G141D	Not applicable
		pme31-2	R363	g182a	Conserved G61E	Not applicable
		pme31-3	R922	g1023a	Conserved G201D	Not applicable

[a] Comparison to description of previously published alleles.

peroxisomal functions, we mutagenized a line expressing GFP-PTS1 and screened 5-day-old seedling hypocotyls for fluorescence distributions that differed from wild type. We examined the progeny of these mutants for additional peroxisome-related defects and identified the causal mutations in 39 mutant lines, revealing 34 novel alleles in 15 genes (Table 1).

Mutations in DRP3A, which encodes a peroxisome division protein

In *Arabidopsis*, three DYNAMIN-RELATED PROTEIN (DRP) GTPases are implicated in peroxisome division: DRP3A (Mano *et al.* 2004), DRP3B (Zhang and Hu 2009), and DRP5B (Zhang and Hu 2010). We recovered two *DRP3A* mutants, *drp3a-4* (R224) and *drp3a-5* (R402), that displayed enlarged peroxisomes and peroxules (Figure 3B). Sequencing *DRP3A* revealed a nonsense mutation at Gln224 in *drp3a-4* (Figure 3A). Recombination mapping of *drp3a-5* indicated linkage at chromosome 4 (Figure 3A), and whole-genome sequencing (Figure 4M, Table S5, and File S1) revealed a *DRP3A* mutation that changed Arg94 to His (Figure 3A). Arg94 is located in the GTPase domain that is conserved in *Arabidopsis* DRPs (Mano *et al.* 2004), plant DRP3 proteins (Hamada *et al.* 2006), *Saccharomyces cerevisiae* Dnm1 (Zhang and Hu 2009), and in close homologs in other organisms (Figure 3A). Previously described mutants in *DRP3A* have enlarged and elongated

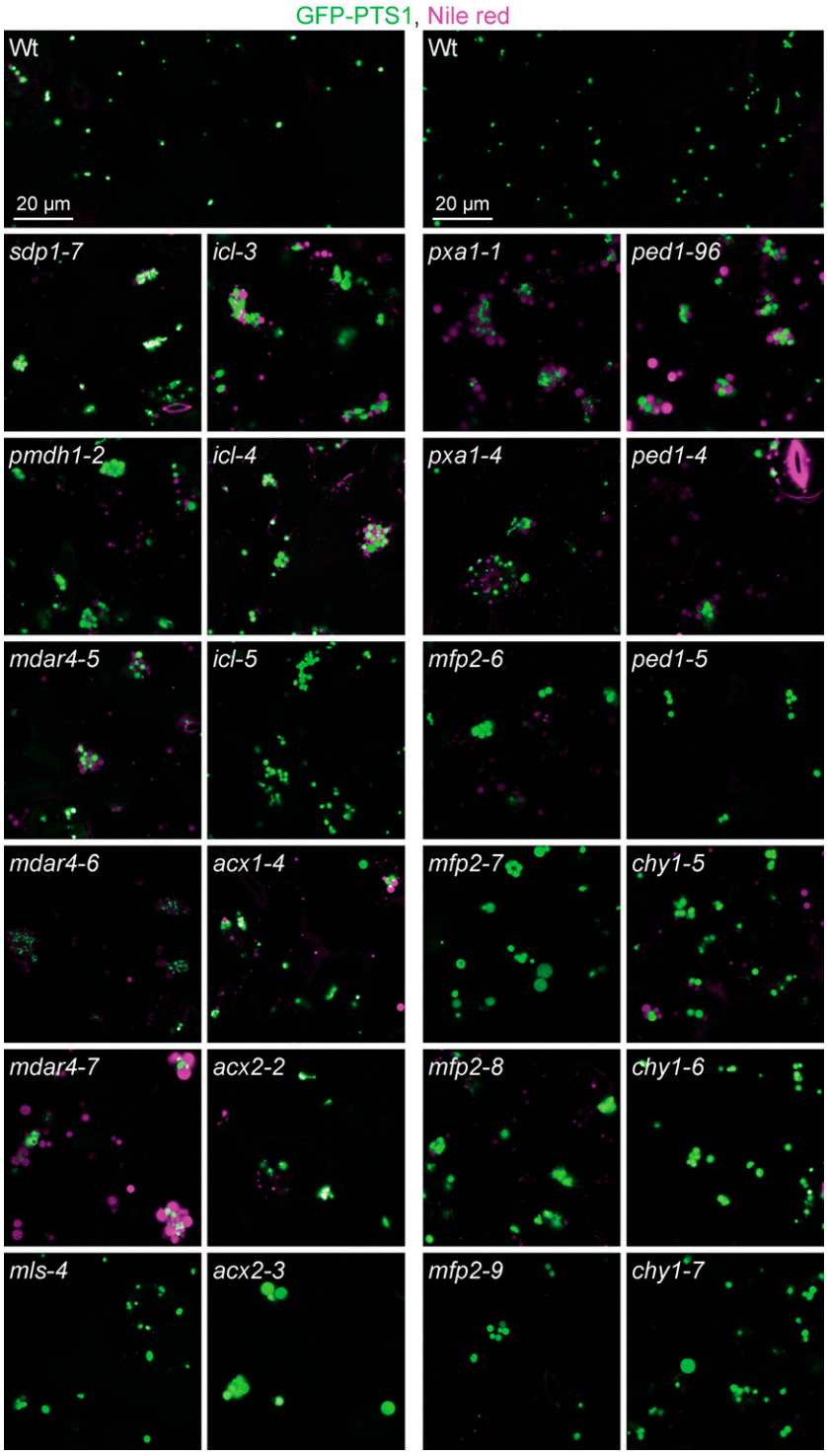

Figure 2 Mutants impaired in lipid mobilization display peroxisomes clustered around retained oil bodies. Confocal micrographs were taken of cotyledon epidermal cells of 4-day-old seedlings expressing peroxisomally targeted fluorescence (GFP-PTS1; green) and stained with Nile red for oil body visualization (magenta). Data are representative of three replicates. Bar, 20 µm.

peroxisomes with numerous peroxules, resulting in a beads-on-a-string pattern (Mano *et al.* 2004; Zhang and Hu 2008; Aung and Hu 2009; Fujimoto *et al.* 2009). Our *drp3a-4* and *drp3a-5* mutants presented enlarged peroxisomes and some peroxules (Figure 3B), but did not show dramatic peroxule overabundance in our growth conditions or examined tissues. *drp3a-4* and *drp3a-5* lacked peroxisome-related physiological defects in IBA or 2,4-DB responsiveness (Figure 3C), similar to previously characterized *drp3a* mutants (Mano *et al.* 2004; Zhang and Hu 2008; Aung and Hu 2009; Fujimoto *et al.* 2009).

Numerous lipid mobilization mutants show peroxisome clustering around oil bodies

Unlike wild-type seedlings, which display evenly distributed peroxisomes, most of our mutants displayed clustered peroxisomes (Figure 2). Cloning the defective genes revealed that

these mutants were directly or indirectly disrupted in fatty acid β-oxidation.

SDP1 is the primary TAG lipase in *Arabidopsis* seedlings (Figure 1; Eastmond 2006). Recombination mapping of the R330 mutant indicated linkage at the top of chromosome 5 (Figure 5A), and whole-genome sequencing (Figure 4A, Table S5, and File S1) revealed a mutation in *SDP1* that changed Arg359 to Trp (*sdp1-7*). Arg359 is conserved in other plants and the yeast TAG lipase Tgl4p (Figure 5A). In addition to having clustered peroxisomes (Figure 2), *sdp1-7* was sensitive to IBA and 2,4-DB (Figure 5D) and retained oil bodies longer than wild type (Figure 2), similar to previously isolated *sdp1* mutants (Eastmond 2006). However, *sdp1-7* was sucrose independent (Figure 5C), unlike previously isolated *sdp1* mutants, which were isolated based on sucrose-dependent growth (Eastmond 2006), suggesting that *sdp1-7* is a partial loss-of-function allele.

Another protein important for oil body mobilization is MONODEHYDROASCORBATE REDUCTASE4 (MDAR4), also known as SDP2, which is part of the membrane-associated ascorbate-dependent electron transfer system that helps detoxify H_2O_2 at the peroxisome surface (Figure 1; Eastmond 2007). Mutations in *MDAR4* lead to increased H_2O_2 levels, decreased SDP1 activity, and sucrose-dependent growth, perhaps because H_2O_2 escapes the peroxisome and inactivates nearby SDP1 (Eastmond 2007). We isolated three novel *mdar4* alleles: *mdar4-5* (R340 and R343), *mdar4-6* (R541 and R577), and *mdar4-7* (R923). Recombination mapping of *mdar4-5* and *mdar4-7* indicated linkage on chromosome 3 (Figure 5E); sequencing *MDAR4* revealed a mutation that changed the conserved Gly122 to Asp in *mdar4-5* and a mutation in the splice acceptor site of the second intron in *mdar4-7* (Figure 5E). Whole-genome sequencing of *mdar4-6* (Figure 4B, Table S5, and File S1) revealed an *MDAR4* mutation that changed conserved Gly11 to Arg (Figure 5E). The *mdar4-6* mutation is in the same codon as the *sdp2-2* mutation that changes Gly11 to Glu (Eastmond 2007). The *mdar4* mutants had clustered peroxisomes around retained oil bodies (Figure 2) and were sucrose dependent (Figure 5F), similar to the previously described *mdar4-4* and other *mdar4* mutants (Eastmond 2007). Additionally, *mdar4* mutants had wild-type IBA and 2,4-DB responsiveness (Figure 5G).

PMDH1 is one of two partially redundant enzymes and accounts for most of the peroxisomal recycling of NADH from fatty acid β-oxidation to NAD^+ (Figure 1; Pracharoenwattana *et al.* 2007). Recombination mapping of the R92 mutant revealed linkage at chromosome 2 (Figure 5B), and whole-genome sequencing (Figure 4C, Table S5, and File S1) revealed a *PMDH1* nonsense mutation (*pmdh1-2*) at Gln129 (Figure 5B). Although *pmdh1-1* was previously reported to be sucrose dependent (Pracharoenwattana *et al.* 2007), *pmdh1-1* and *pmdh1-2* were sucrose independent in our growth conditions (Figure 5C). *pmdh1-2* was 2,4-DB resistant (Figure 5D), similar to *pmdh1-1* (Figure 5D; Pracharoenwattana *et al.* 2007), whereas neither *pmdh1-1* nor *pmdh1-2* displayed IBA resistance (Figure 5D). Additionally, the *pmdh1-2* single mutant retained oil bodies (Figure 2) as reported for the *pmdh1-1 pmdh2-1* double mutant (Pracharoenwattana *et al.* 2007).

PXA1 imports fatty acids into the peroxisome (Figure 1). Whole-genome sequencing of the R751 mutant (Figure 4H and Table S5) revealed a *PXA1* mutation (*pxa1-4*) that changed Gly307 to Glu. Gly307 is located within an EAA-like motif ($EAAX_3GX_9IXLP$) that is similar to fatty-acid-binding domains (Shani *et al.* 1995) and is conserved in plants, yeast, and humans (Figure 6A; Zolman *et al.* 2001b). In *S. cerevisiae*, a mutation in the equivalent Gly413 in Pxa1p (Figure 6A) impairs fatty acid β-oxidation (Shani *et al.* 1996). Mutations in the equivalent Gly298 in a human PXA1 homolog (Figure 6A) cause adrenomyeloneuropathy (Wichers *et al.* 1999) or Addison's disease (Lachtermacher *et al.* 2000). *pxa1-4* was sucrose dependent and IBA and 2,4-DB resistant (Figure 6, D and E), resembling *pxa1-1* and other *pxa1* mutants (Zolman *et al.* 2001b; Footitt *et al.* 2002; Hayashi *et al.* 2002; Dietrich *et al.* 2009). Like previously described *pxa1* mutants (Footitt *et al.* 2002; Dietrich *et al.* 2009), *pxa1-4* seedlings retained oil bodies longer than wild type (Figure 2). Therefore, Gly307 appeared to be important for import of fatty acids and IBA in *Arabidopsis*, supporting previous yeast data suggesting that the EAA-like motif is important for substrate recognition (Shani *et al.* 1995). However, the EAA-like motif did not seem to be critical for germination, because germination defects were not noticed in mutants with alterations in the EAA-like motif (Dietrich *et al.* 2009), including *pxa1-4*. In contrast, the strong *comatose* alleles of *pxa1* have clear germination defects (Russell *et al.* 2000; Footitt *et al.* 2002; Dietrich *et al.* 2009). As with previously described alleles, *pxa1-4* processed PTS2 proteins like wild type (Figure 6F).

ACX1 and ACX2 are partially redundant enzymes that catalyze the first step of fatty acid β-oxidation (Figure 1). Whole-genome sequencing of R574 (Figure 4I, Table S5, and File S1) revealed an *ACX1* mutation that changed Gly226 to Arg (*acx1-4*). Gly226 is conserved in ACX1 homologs in other organisms (Figure 6B). *acx1-4* processed PTS2 proteins like wild type (Figure 6F) and was sucrose independent and IBA resistant (Figure 6, D and E), similar to *acx1-2* and other previously isolated *acx1* mutants (Adham *et al.* 2005; Pinfield-Wells *et al.* 2005). *acx1-4* and *acx1-2* were 2,4-DB resistant in our conditions (Figure 6E), unlike a previous report of *acx1-2* having wild-type 2,4-DB responsiveness (Pinfield-Wells *et al.* 2005). *acx1-4* had clustered peroxisomes with some oil body retention (Figure 2), unlike previously characterized *acx1* mutants that display wild-type peroxisome distribution (Pinfield-Wells *et al.* 2005).

We recovered two new *acx2* mutations. Recombination mapping of *acx2-2* (R233) and *acx2-3* (R737) revealed linkage at the bottom of chromosome 5 (Figure 6C). Sequencing *ACX2* revealed a mutation in *acx2-2* that would convert Trp154 to a premature stop codon and an adjacent mutation in *acx2-3* that would change Gly155 to Arg. Gly155 is conserved in ACX2 homologs of other organisms (Figure 6C).

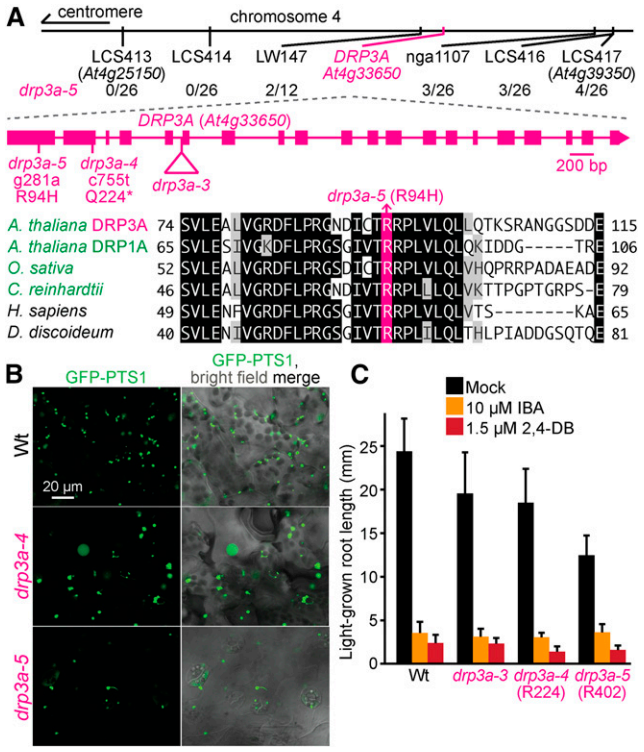

Figure 3 Mutations in *DRP3A* confer enlarged peroxisomes. (A) Chromosome map indicates the positions of markers used to map *drp3a-5* and ratios of recombinants to the number of chromosomes assessed. A gene diagram indicates the position of *drp3a* mutations. DRP3A was aligned with related proteins (Table S4); residues are shaded when identical (black or pink) or chemically similar (gray) in at least four sequences. (B) Confocal micrographs were taken of cotyledon epidermal cells of 8-day-old seedlings expressing peroxisomally targeted fluorescence (GFP-PTS1; green). (C) Root lengths of 8-day-old seedlings were measured. Error bars show SD (n = 20). Data (B, C) are representative of three replicates. Bar, 20 μm.

acx2-2 and *acx2-3* processed PTS2 proteins like wild type (Figure 6F) and were sucrose independent and IBA and 2,4-DB sensitive (Figure 6, D and E), similar to *acx2-1* (Adham *et al.* 2005; Pinfield-Wells *et al.* 2005). *acx2-2* and *acx2-3* displayed clustered peroxisomes around retained oil bodies (Figure 2), whereas *acx2-1* accumulates acyl-CoA but displays normal peroxisome distribution with no oil body retention (Pinfield-Wells *et al.* 2005).

MFP2 catalyzes the second and third steps of fatty acid β-oxidation (Figure 1). We found five mutants carrying four different *MFP2* mutations: *mfp2-6* (R281), *mfp2-7* (R778), *mfp2-8* (R794 and R809), and *mfp2-9* (R1009). Sequencing *MFP2* following recombination mapping to chromosome 3 revealed mutations that changed Gly670 to Arg in *mfp2-6*, Gly320 to Asp in *mfp2-8*, and Glu342 to Lys in *mfp2-9* (Figure 7A). Whole-genome sequencing revealed the same Gly320Asp mutation in a different *mfp2-8* isolate (Figure 4K, Table S5, and File S1) and an Ala454-to-Thr mutation in *mfp2-7* (Figure 4J, Table S5, and File S1). All four mutations alter conserved residues in the MFP2 C-terminal dehydrogenase domain (Figure 7A). Gly320 is between two residues important for NAD^+ binding (Arent *et al.* 2010), and Ala454 follows two conserved residues, Ser452 and Pro453, that facilitate substrate orientation in *Arabidopsis* MFP2 (Arent *et al.* 2010). *mfp2-6*, *mfp2-8*, and *mfp2-9* were partially sucrose dependent and IBA and 2,4-DB sensitive (Figure 7, D and E), and displayed clustered peroxisomes around accumulated oil bodies (Figure 2), like previously characterized *mfp2* mutants (Rylott *et al.* 2006). *mfp2-7* also showed clustered peroxisomes around retained oil bodies but, in contrast to the other *mfp2* alleles, *mfp2-7* was sucrose independent and displayed slight 2,4-DB resistance (Figure 7, D and E).

PED1 is a 3-ketoacyl-CoA thiolase that catalyzes the last step of fatty acid β-oxidation (Figure 1). Sequencing *PED1* in several mutants revealed mutations changing Gly109 to Glu in *ped1-4* (R814) and Gly141 to Asp in *ped1-5* (R883). Gly109 and Gly141 are conserved in plants and homologs in humans and yeast (Figure 7B). *ped1-5* displayed reduced levels of protein detected with an anti-thiolase antibody (Figure 11A), peroxisomes clustered around retained oil bodies (Figure 2), sucrose dependence, and IBA- and 2,4-DB resistance (Figure 7, D and E). These phenotypes were similar to those of *ped1-96* (Lingard and Bartel 2009) and other previously characterized *ped1* mutants (Hayashi *et al.* 1998; Germain *et al.* 2001; Lingard and Bartel 2009; Burkhart *et al.* 2013; Wiszniewski *et al.* 2014). Although *ped1-4* displayed robust sucrose dependence (Figure 7D) and 2,4-DB resistance (Figure 7E), this allele was sensitive to IBA (Figure 7E). The less severe defects observed in *ped1-4* suggest that ped1-4 protein, which accumulates at wild-type levels (Figure 11A), retains partial function.

Mutations in *CHY1* confer *ped1*-like phenotypes (Zolman *et al.* 2001a). We recovered three *chy1* mutants that displayed peroxisomes clustered around retained oil bodies (Figure 2). Recombination mapping indicated linkage at the bottom of chromosome 5 (Figure 7C), and sequencing *CHY1* revealed mutations that changed Gly119 to Asp in *chy1-5* (R189), Asp150 to Asn in *chy1-6* (R499 and R506), and Gly165 to Glu in *chy1-7* (R728). Asp150 is needed for *in vitro* CHY1 enzymatic activity (Zolman *et al.* 2001a), and all three mutations altered residues conserved among closely related genes in *Arabidopsis* and humans (Zolman *et al.* 2001a) and other species (Figure 7C). *chy1-5*, *chy1-6*, and *chy1-7* were sucrose dependent, IBA resistant, and 2,4-DB resistant (Figure 7, D and E), similar to *chy1-1* and other previously characterized *chy1* mutants (Zolman *et al.* 2001a; Lange *et al.* 2004).

We also recovered several mutants disrupted in the glyoxylate cycle. We isolated three *icl* mutants with peroxisomes clustered around retained oil bodies (Figure 2). Recombination mapping of *icl-4* (R601) indicated linkage at chromosome 3 (Figure 8A), and whole-genome sequencing of *icl-3* (R291) and *icl-4* (Figure 4, D and E, Table S5, and File S1) revealed *ICL* mutations that changed Glu21 to Lys in *icl-3* and Gly84 to Arg in *icl-4* (Figure 8A). Glu21 is conserved in plant ICL homologs, and Gly84 is conserved in plants and yeast

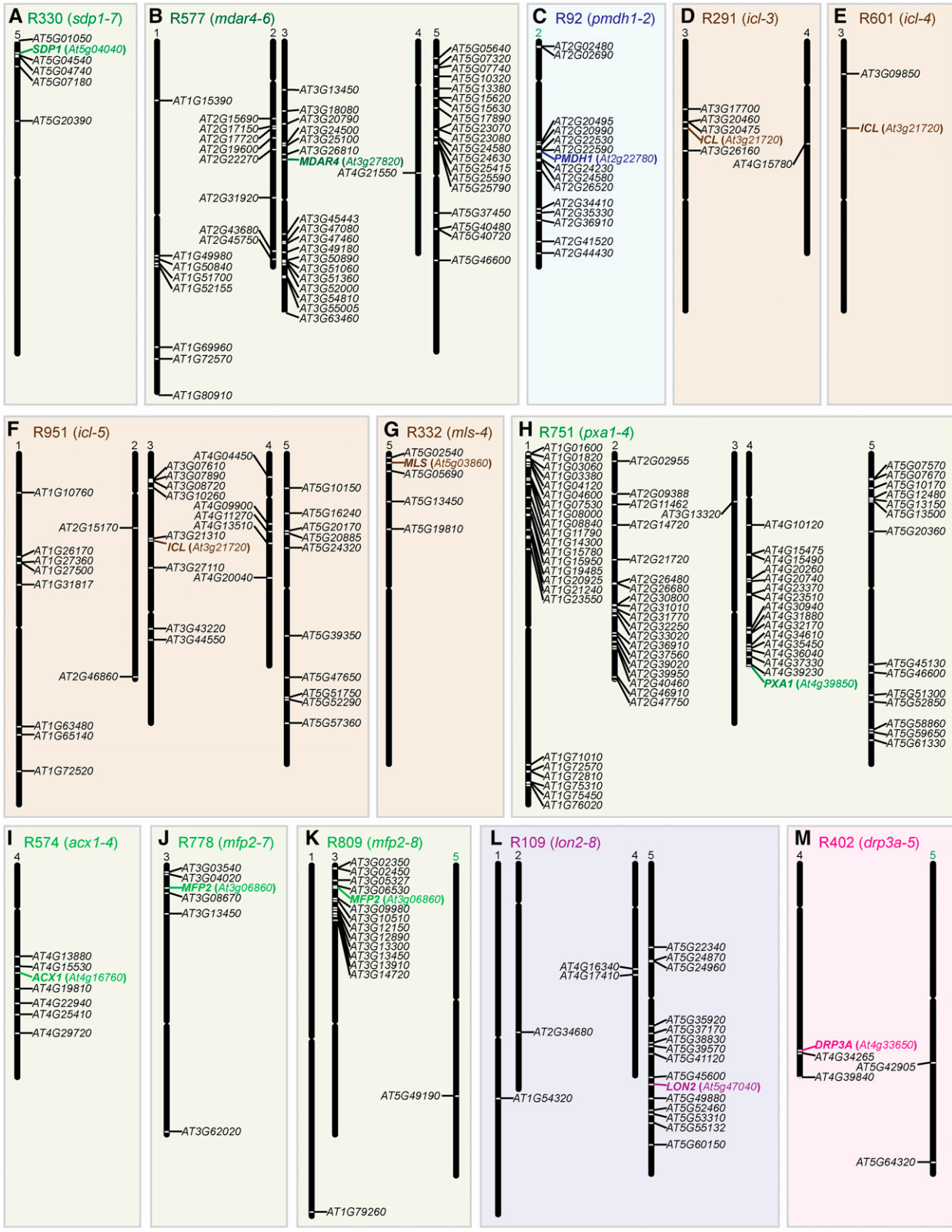

Figure 4 Mutations identified through whole-genome sequencing in the isolated mutants. Chromosome maps (A–M) indicate the positions and gene identifier numbers of genes with homozygous EMS-consistent changes in splice sites or nonsynonymous amino acid changes in coding regions. Chromosomes that are not shown lacked such mutations. Presumptive causal mutations are denoted in color. Results for *mdar4-6* (R541) are not shown because only a single homozygous EMS-consistent mutation (*mdar4-6*) was found (File S1).

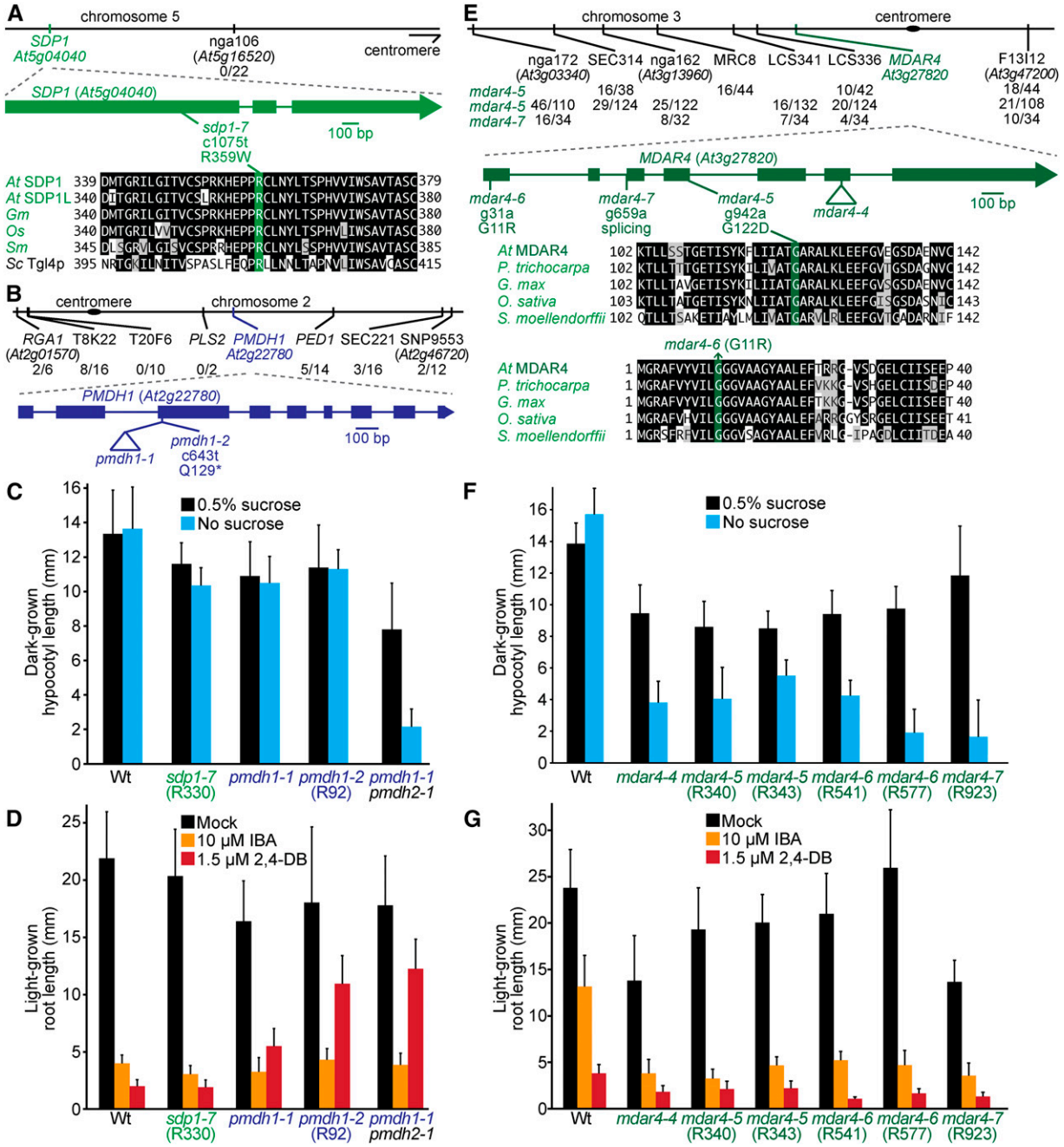

Figure 5 A mutation in *SDP1* that does not cause physiological defects, mutations in *MDAR4* confer sucrose dependence, and mutations in *PMDH1* confer 2,4-DB resistance. (A, B) Chromosome maps indicate the positions of markers used to map *sdp1-7* (A) and *pmdh1-2* (B) mutants and ratios of recombinants to the number of chromosomes assessed. Gene diagrams indicate the positions of the *sdp1-7* (A) and *pmdh1* (B) mutations. SDP1 was aligned (A) with related proteins (Table S4); residues are shaded when identical (black or green) or chemically similar (gray) in at least four sequences. (C) Hypocotyl lengths of 5-day-old dark-grown seedlings were measured. Error bars show SD (n = 20). (D) Root lengths of 8-day-old light-grown seedlings were measured. Error bars show SD (n = 20). (E) Chromosome map indicates the positions of markers used to map *mdar4* mutations and ratios of recombinants to the number of chromosomes assessed. A gene diagram indicates the positions of *mdar4* mutations. MDAR4 was aligned with related proteins (Table S4); residues are shaded when identical (black or green) or chemically similar (gray) in at least three sequences. (F) Hypocotyl lengths of 5-day-old dark-grown seedlings were measured. Error bars show SD (n = 20). (G) Root lengths of 8-day-old light-grown seedlings were measured. Error bars show SD (n = 20). Data are representative of two (C, F) or three (D, G) replicates.

(Figure 8A). Whole-genome sequencing of *icl-5* (R951) (Figure 4F, Table S5, and File S1) revealed an *ICL* nonsense mutation at Trp371 (Figure 8A). Like *icl-1*, ICL protein was not detected in the *icl-5* nonsense allele. In contrast, both missense alleles accumulated icl protein, although icl-3 had a slight shift in electrophoretic mobility (Figure 8C). Like *icl-1* (Eastmond *et al.* 2000a), all *icl* alleles responded like wild type to IBA and 2,4-DB (Figure 8E), and *icl-5* was

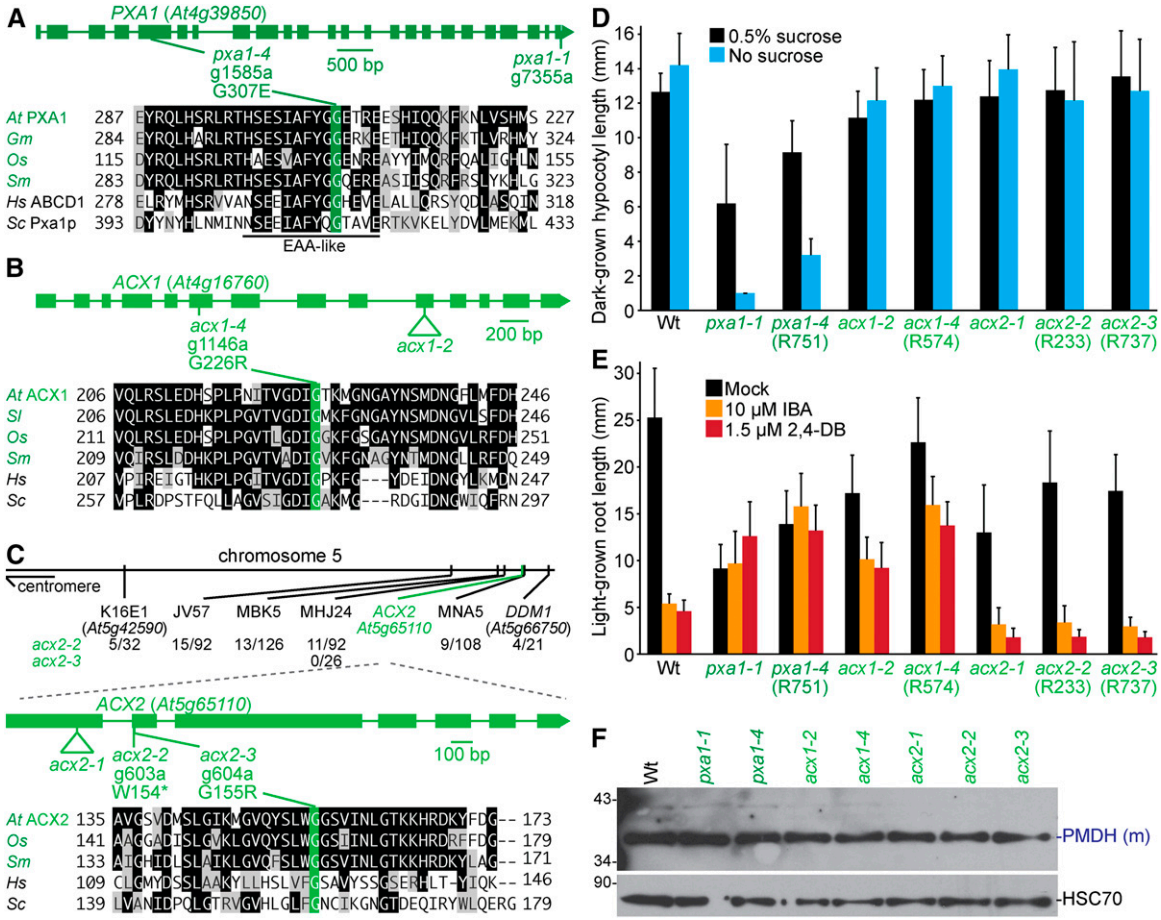

Figure 6 Mutations in *PXA1* confer sucrose dependence and IBA and 2,4-DB resistance, and mutations in *ACX1* lead to IBA and 2,4-DB resistance, whereas mutations in *ACX2* do not generate notable physiological defects. (A–C) Gene diagrams indicate positions and nature of *pxa1* (A), *acx1* (B), and *acx2* (C) mutations. PXA1 (A), ACX1 (B), and ACX2 (C) were aligned with related proteins (Table S4); residues are shaded when identical (black or green) or chemically similar (gray) in at least four (A, B) or three (C) sequences. Chromosome map indicates the positions of markers used to map *acx2* mutants and ratios of recombinants to the number of chromosomes assessed (C). (D) Hypocotyl lengths of 5-day-old dark-grown seedlings were measured. Error bars show SD (n = 20). (E) Root lengths of 8-day-old light-grown seedlings were measured. Error bars show SD ($n \geq 14$). Data are representative of two (D) or three (E) replicates. (F) Eight-day-old seedlings were prepared for immunoblot analysis and serially probed with antibodies recognizing the indicated proteins. PMDH is translated as a precursor with a PTS2 that is cleaved in the peroxisome to yield mature (m) protein. HSC70 was used as a loading control. Positions of molecular mass markers (in kDa) are indicated on the left.

sucrose-dependent in the dark (Figure 8D). In contrast, *icl-3* and *icl-4* were sucrose independent (Figure 8D). The sucrose independence of *icl-3* and *icl-4* suggests that the icl protein that accumulates in these mutants (Figure 8C) retains partial function.

We recovered a mutant in *MLS*, *mls-4* (R332), with clustered peroxisomes (Figure 2). Recombination mapping indicated linkage at chromosome 5 (Figure 8A), and whole-genome sequencing (Figure 4G, Table S5, and File S1) revealed an *MLS* mutation in the splice acceptor site of the third intron (Figure 8B). Immunoblot analysis of MLS protein revealed reduced levels and faster electrophoretic mobility of mls-4 (Figure 8C). *mls-4* was slightly sucrose dependent, similar to the null *mls-3* allele (Figure 8D) and other *mls* mutants (Cornah *et al.* 2004). *mls-3* and *mls-4* were IBA and 2,4-DB sensitive (Figure 8E).

These *sdp1*, *pmdh1*, *mdar4*, *pxa1*, *acx1*, *acx2*, *mfp2*, *ped1*, *chy1*, *icl*, and *mls* mutants were originally selected for clustered GFP-PTS1 puncta, and confocal microscopy revealed that peroxisomes were clustered around retained oil bodies (Figure 2). Because the mutations identified are in genes directly or indirectly implicated in lipid mobilization, we concluded that these mutants were isolated due to delayed lipid mobilization, which led to peroxisomes clustering around retained oil bodies.

Fatty acid β-oxidation mutants have defects in peroxisome size and matrix protein import

Several fatty acid β-oxidation mutants displayed peroxisomal defects beyond the physiological phenotypes expected from impaired β-oxidation (sucrose dependence and IBA or 2,4-DB resistance). For example, *acx1-4*, *acx2-2*, and *acx2-3* displayed some enlarged peroxisomes (Figure 9, C and D) similar to the *acx1-2 acx2-1* double mutant (Pinfield-Wells *et al.* 2005), but unlike previously characterized *acx1* and

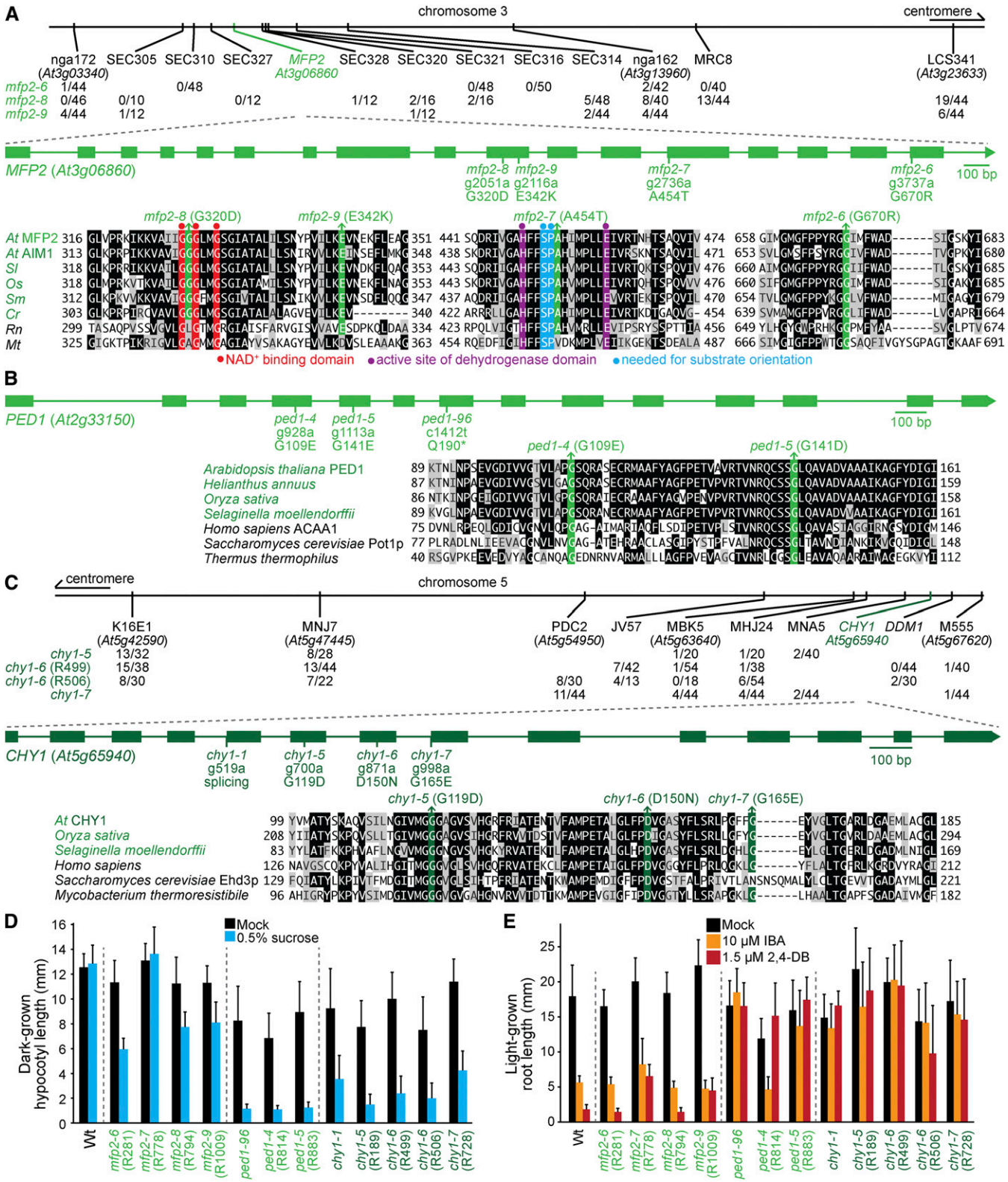

Figure 7 Mutations in *MFP2*, *PED1*, and *CHY1* confer sucrose dependence and IBA and 2,4-DB resistance. (A–C) Chromosome map indicates the positions of markers used to map *mfp2* (A) and *chy1* (C) mutants and ratios of recombinants to the number of chromosomes assessed. Gene diagrams indicate the position of *mfp2* (A), *ped1* (B), and *chy1* (C) mutations. MFP2 (A), PED1 (B), and CHY1 (C) were aligned with related proteins (Table S4); residues are shaded when identical (black or colors) or chemically similar (gray) in at least five (A) or four (B, C) sequences. (D) Hypocotyl lengths of 5-day-old dark-grown seedlings were measured. Error bars show SD ($n = 20$). (E) Root lengths of 8-day-old light-grown seedlings were measured. Error bars show SD ($n \geq 15$). Data are representative of three replicates (D, E).

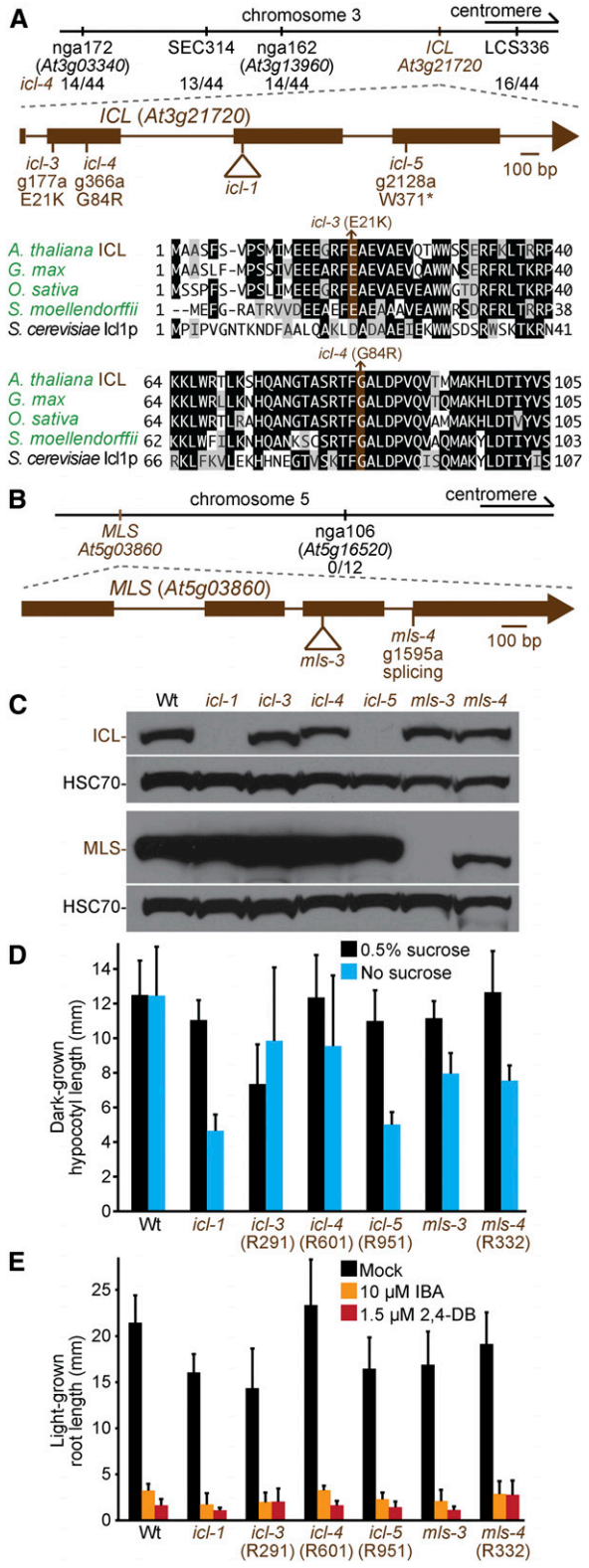

Figure 8 Mutations in *ICL* and *MLS* confer sucrose dependence. (A, B) Chromosome maps indicate the positions of markers used to map *icl-4* (A) or *mls-4* (B) and ratios of recombinants to the number of chromosomes assessed. Gene diagrams indicate the positions of *icl* (A) or *mls* (B) mutations. ICL was aligned (A) with related proteins (Table S4); residues are shaded when identical (black or brown) or chemically similar (gray) in at least three sequences. (C) Eight-day-old seedlings were used for immunoblot analysis and serially probed with antibodies recognizing the indicated proteins. HSC70 was used as a loading control. (D) Hypocotyl lengths of 5-day-old dark-grown seedlings were measured. Error bars show SD (n = 20). (E) Root lengths of 8-day-old light-grown seedlings were measured. Error bars show SD (n = 20). Data are representative of two replicates (C, D).

acx2 single mutants, which have wild-type-sized peroxisomes (Pinfield-Wells *et al.* 2005). Additionally, some peroxisomes were enlarged in *mfp2-6*, *mfp2-7*, *mfp2-8*, *mfp2-9*, *ped1-4*, and *ped1-5* (Figure 9, E and F), similar to previously isolated *mfp2* (Rylott *et al.* 2006) and *ped1* (Hayashi *et al.* 1998; Germain *et al.* 2001) mutants. Moreover, *chy1-5*, *chy1-6*, and *chy1-7* had some enlarged peroxisomes (Figure 9G), which had not been reported previously.

Unlike in mutants with impaired fatty acid β-oxidation enzymes, peroxisome size resembles wild type in *pxa1* mutants (Footitt *et al.* 2002), including our *pxa1-4* allele (Figure 9B), and in *lacs6-1 lacs7-1* (Fulda *et al.* 2004). PXA1 interacts physically and functionally with LACS6/7 in yeast (De Marcos Lousa *et al.* 2013), so PXA1 transport may be reduced in the *lacs6-1 lacs7-1* mutant. Other mutants blocked early in lipid mobilization, such as *sdp1* and *mdar4*, which indirectly reduces SDP1 activity (Eastmond 2007), also displayed wild-type-sized peroxisomes (Figure 2). Thus, fatty acid mobilization defects upstream of fatty acid import appear not to cause peroxisome enlargement. Fatty acid mobilization defects downstream of fatty acid import do lead to enlarged peroxisomes (Table 2), suggesting that excessive peroxisomal fatty acids or their β-oxidation intermediates cause peroxisome enlargement in β-oxidation mutants (Graham *et al.* 2002).

We also observed that a subset of peroxisomes in wild type cotyledons became transiently enlarged around 4 days after plating (Figure 10). The numerous oil bodies in germinating cotyledons became less abundant during the first 4 days of development as peroxisomes enlarged (Figure 10). By day 5, few oil bodies remained, and peroxisomes returned to the original size (Figure 10). This transient enlargement of a subset of peroxisome in wild type during oil body consumption is consistent with the hypothesis that fatty acids can overwhelm the β-oxidation machinery, leading to peroxisomal accumulation of fatty acids or β-oxidation intermediates, a state similar to the one expected in fatty acid β-oxidation mutants with enlarged peroxisomes.

Fatty acid β-oxidation mutants also displayed peroxisomal matrix protein import defects. *mfp2-6*, *mfp2-8*, and *ped1-4* mislocalized some GFP-PTS1 to the cytosol (Figure 9, E and F) similarly to *ped1-96* (Figure 9F), which also mislocalizes GFP-ICL (Burkhart *et al.* 2013). Furthermore, immunoblot analysis revealed that *mfp2-6*, *mfp2-8*, *ped1-4*, *ped1-5*, *chy1-1*, and *chy1-5* seedlings displayed partial PTS2-processing defects (Figure 11A) similar to *ped1-96* (Burkhart *et al.* 2013). In contrast, *pxa1*, *acx1*, and *acx2* mutants displayed wild-type PTS2-processing (Figure 11A).

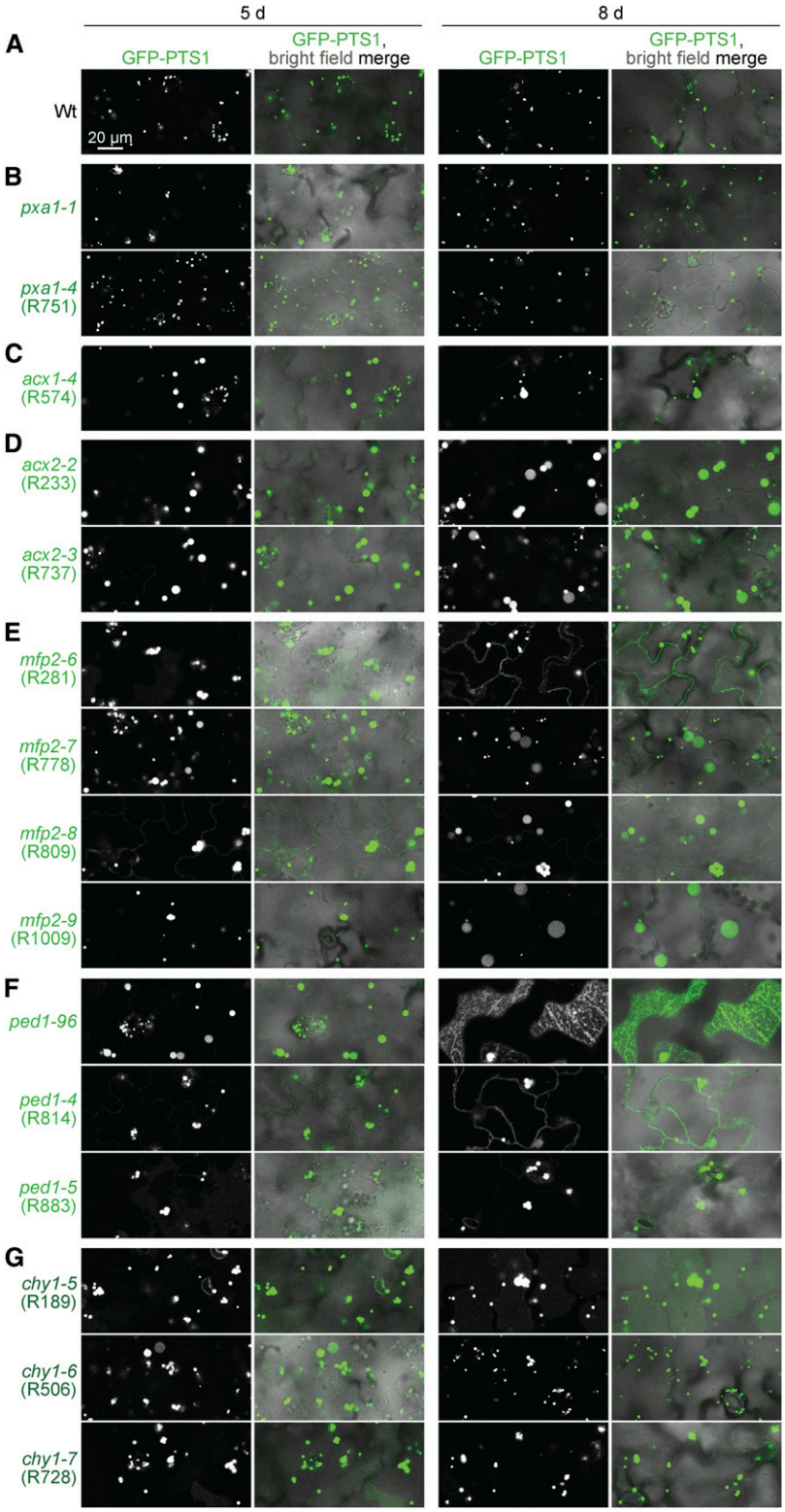

Figure 9 A subset of fatty acid β-oxidation mutants display enlarged peroxisomes and matrix protein import defects. (A–G) Wild type (A) and *pxa1* mutants (B) display small peroxisomes, whereas mutations in *ACX1* (C), *ACX2* (D), *MFP2* (E), *PED1* (F), and *CHY1* (G) lead to enlarged peroxisomes and some GFP-PTS1 mislocalization to the cytosol. Confocal micrographs were taken of cotyledon epidermal cells of 5- or 8-day-old seedlings expressing peroxisomally targeted fluorescence (GFP-PTS1; white in left panels; green in merged images). Data are representative of three replicates. Bar, 20 μm.

Like *ped1* mutants, *chy1* mutants displayed enlarged peroxisomes, cytosolic GFP-PTS1 mislocalization, and PTS2-processing defects (Figure 9G and Figure 11, A and D). In *chy1* mutants, methacrylyl-CoA is thought to accumulate and inactivate the PED1 thiolase, yielding *ped1*-like defects (Zolman *et al.* 2001a; Lange *et al.* 2004). Isobutyrate is an intermediate upstream of methacrylyl-CoA (Figure 1), and *chy1* root elongation is hypersensitive to isobutyrate (Lucas *et al.* 2007), perhaps because isobutyrate supplementation further increases methacrylyl-CoA levels. To determine if

Table 2 Summary of peroxisome size and import defects in fatty acid β-oxidation mutants

Mutant	Defect	Peroxisome size	PTS2 processing	PTS1 import
pxa1	Fatty acid import into peroxisomes	Wt[a]	Wt[b]	Wt[b]
lacs6-1 lacs7-1	Fatty acid import and activation	Wt[c]	Not determined	Not determined
acx1-2 acx2-1	Fatty acid β-oxidation	Large[d]	Not determined	Not determined
mfp2	Fatty acid β-oxidation	Large[e]	Defect[b]	Defect[b]
ped1	Fatty acid β-oxidation	Large[f]	Defect[g]	Defect[g]
pxn	NAD^+ and CoA import into peroxisomes	Large[h]	Wt[b]	Wt[b]
pxa1 pxn	Fatty acid, NAD^+, and CoA import into peroxisomes	Wt[b]	Wt[b]	Wt[b]
pxn ped1	NAD^+ and CoA import into peroxisomes and fatty acid β-oxidation	Large[b]	Enhanced defect[b]	Enhanced defect[b]

[a] This work and Hayashi *et al.* (2002).
[b] This work.
[c] Fulda *et al.* (2004).
[d] Pinfield-Wells *et al.* (2005).
[e] This work and Rylott *et al.* (2006).
[f] This work and Hayashi *et al.* (1998).
[g] This work and Burkhart *et al.* (2013).
[h] This work and Mano *et al.* (2011).

PED1 inhibition by methacrylyl-CoA was solely responsible for *chy1* mutant defects, we supplemented the growth medium with isobutyrate. We found that growth on isobutyrate appeared to slightly increase peroxisome size in 8-day-old wild-type seedlings while markedly enhancing peroxisome enlargement, oil body retention, and peroxisome clustering around retained oil bodies in the *chy1-6* mutant (Figure 11C). Isobutyrate enhanced the PTS2-processing defect in *chy1-1* and *chy1-6* without impairing PTS2 processing in wild type (Figure 11D). Interestingly, isobutyrate conferred a more severe PTS2-processing defect on *chy1* than on the *ped1-96* null mutant (Figure 11D), suggesting that methacrylyl-CoA has additional targets beyond PED1 that affect PTS2 processing.

LON PROTEASE2 AAA⁺ ATPase domain is needed for function

LON PROTEASE2 (LON2) is a peroxisomal protein that belongs to a family of **A**TPases **a**ssociated with diverse cellular **a**ctivities$^+$ (AAA^+) and is needed for sustained peroxisome function during seedling development (Lingard and Bartel 2009). We recovered three mutants with enlarged GFP-PTS1 puncta accompanied by some cytosolic GFP-PTS1 fluorescence reminiscent of *lon2* mutants (Farmer *et al.* 2013; Goto-Yamada *et al.* 2014). Sequencing *LON2* revealed a nonsense mutation at Trp45 in *lon2-10* (R973) and a mutation that changed Arg537 to Lys in *lon2-9* (R498; Figure 12A). Recombination mapping of R109 using the enlarged puncta phenotype failed to identify a clear linkage. Because the enlarged GFP-PTS1 puncta could be due to a *PXN* mutation (Mano *et al.* 2011), we sequenced *PXN* and discovered *pxn-4*. However, R109 also presented IBA resistance, cytosolic GFP-PTS1, and a PTS2-processing defect, phenotypes not associated with other *pxn* alleles. Recombination mapping using PTS2-processing defects revealed a linkage at the bottom of chromosome 5 (Figure 12A). Whole-genome sequencing of pooled backcrossed lines with PTS2-processing defects (Figure 4L, Table S5, and File S1) revealed *lon2-8*, a nonsense mutation at Gln102 (Figure 12A). A backcrossed *lon2-8* line homozygous for wild-type *PXN* was used for *lon2-8* assays.

Previously isolated *lon2* mutants display slight sucrose dependence and IBA resistance in root elongation, strong IBA resistance in lateral root promotion, PTS2-processing defects, partially cytosolic localization of peroxisomal matrix proteins (Lingard and Bartel 2009), and dramatically enlarged peroxisomes (Farmer *et al.* 2013; Goto-Yamada *et al.* 2014). Similarly, *lon2-8* and *lon2-10*, which are expected to result in early truncations of LON2 protein, displayed GFP-PTS1 in enlarged puncta and in cytosolic-like distribution (Figure 12B), PTS2-processing defects (Figure 12D), and IBA resistance in lateral root production (Figure 12G), but only slight sucrose dependence (Figure 12E) and minor IBA and 2,4-DB resistance in root elongation (Figure 12F). Interestingly, *lon2-9* also showed a marked GFP-PTS1 mislocalization and enlarged GFP-PTS1 puncta comparable to *lon2* mutants expected to be null alleles (Figure 12B; Goto-Yamada *et al.* 2014), but, in contrast, appeared to process PTS2 proteins normally (Figure 12D) and displayed only slight IBA resistance in lateral root production (Figure 12G), indicating that this missense allele retains some LON2 function.

Fatty acid metabolism is necessary for enlarged puncta in PXN mutants

We identified five mutants with enlarged GFP-PTS1 puncta similar to *pxn* mutants (Mano *et al.* 2011), revealing four new *PXN* mutations: *pxn-4* (R109), *pxn-5* (R162), *pxn-6* (R986), and *pxn-7* (R987 and R995; Figure 12C). Unlike wild type, *pxn* peroxisomes can be large enough to be visible even using bright field microscopy (Figure 13C). Sequencing *PXN* revealed that *pxn-5* had a nonsense mutation at Arg258,

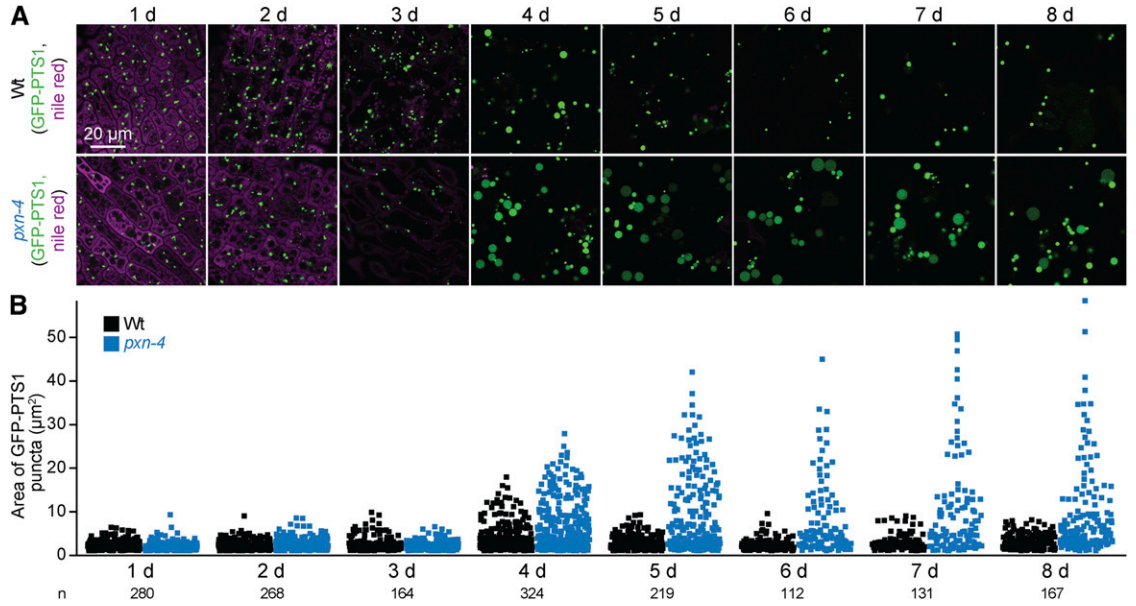

Figure 10 Peroxisomes expand transiently during wild-type seedling development but remain large in *pxn* seedlings. (A) Confocal micrographs were taken of cotyledon epidermal cells of wild-type and *pxn-4* seedlings expressing peroxisomally targeted fluorescence (GFP-PTS1; green) and stained with Nile red for oil body visualization (magenta). (B) GFP-PTS1 puncta areas from one to three 135 × 135 μm images including those shown in (A) are plotted; the number of puncta measured for each genotype is indicated below the *y*-axis labels. The number of puncta per cell was not quantified. Bar, 20 μm.

pxn-6 had a mutation in the splice acceptor sequence of the sixth intron, and *pxn-7* had a mutation in the splice donor site of the ninth exon. *pxn-4* had a mutation in the splice acceptor sequence of the ninth *PXN* intron, and a backcrossed line without *lon2-8* was used for assays. Our *pxn* mutants lacked noticeable matrix protein import defects; they efficiently processed PTS2 proteins (Figure 12D) and lacked cytosolic GFP-PTS1 fluorescence (Figure 12B). *pxn* mutants were sucrose independent (Figure 12E) and sensitive to IBA and 2,4-DB (Figure 12, F and G), similar to wild type and previously characterized *pxn* mutants, which are sucrose independent (Mano *et al.* 2011; Bernhardt *et al.* 2012) and only slightly (Bernhardt *et al.* 2012) or not at all (Mano *et al.* 2011) 2,4-DB resistant. We did not observe *pxn* oil body retention in our conditions (Figure 10), unlike previously characterized *pxn* mutants (Bernhardt *et al.* 2012).

Because one of our mutants, R109, carried both *lon2-8* and *pxn-4* mutations, we examined the double mutant to see if the effects of these mutations were additive. We found that *lon2-8 pxn-4* did not show a further increase in peroxisome size compared to the single mutants (Figure 12B), and that PTS2-processing remained impaired in *lon2-8 pxn-4* (Figure 12D).

The large GFP-PTS1 puncta in *pxn* mutants resemble the enlarged GFP-PTS1 puncta observed in *lon2* mutants (Figure 12B; Farmer *et al.* 2013). LON2 research provided the first evidence of peroxisome-specific autophagy (pexophagy) in plants (Farmer *et al.* 2013). Autophagy is a process that degrades entire organelles and other cellular constituents (reviewed in Li and Vierstra 2012). Combining *lon2* with null mutations in *AUTOPHAGY RELATED* (*ATG*) *2*, *ATG3*, or *ATG7* rescues *lon2* defects, improving peroxisomal matrix protein import, returning peroxisomes to a wild-type size, and stabilizing peroxisomal proteins that are more quickly degraded in *lon2* (Farmer *et al.* 2013; Bartel *et al.* 2014; Goto-Yamada *et al.* 2014; Young and Bartel 2015). We asked if autophagy was similarly required to generate enlarged peroxisomes in *pxn* mutants by crossing *pxn-4* to *atg7-3*, a null autophagy mutant (Lai *et al.* 2011). Whereas *lon2-2 atg7* PTS2-GFP puncta resemble peroxisomes in wild type and *atg7* mutants (Figure 13A; Farmer *et al.* 2013), the *pxn-4 atg7-3* double mutant displayed both large *pxn*-like GFP-PTS1 puncta and smaller puncta (Figure 13A). The additional small GFP-PTS1 puncta observed in *pxn-4 atg7-3* (Figure 13A) may reflect accumulating peroxisomes caused by autophagy disruption in *atg7-3*. We concluded that the mechanism by which peroxisomes increase in size in *pxn* does not involve pexophagy and is distinct from the mechanism that generates large GFP-PTS1 puncta in *lon2-2*.

The enlarged peroxisomes in *pxn* mutants might relate to the role of PXN in importing NAD^+ (Agrimi *et al.* 2012; Bernhardt *et al.* 2012; van Roermund *et al.* 2016), a key cofactor in fatty acid β-oxidation (Figure 1). Perhaps in *pxn* mutant peroxisomes, oxidized NAD^+ is depleted and fatty acid β-oxidation stalls. This situation would resemble that of fatty acid β-oxidation mutants that show enlarged peroxisomes (Figure 9, C–G). We examined *pxn* peroxisomes following germination, when fatty acids might accumulate in peroxisomes due to intense lipid mobilization. We found that *pxn* peroxisomes were similar in size to wild-type peroxisomes during the first few days after germination, starting small and enlarging by 4 days (Figure 10). However, wild-type peroxisomes returned to a normal size at day 5, when visible oil bodies had been consumed, while numerous *pxn*

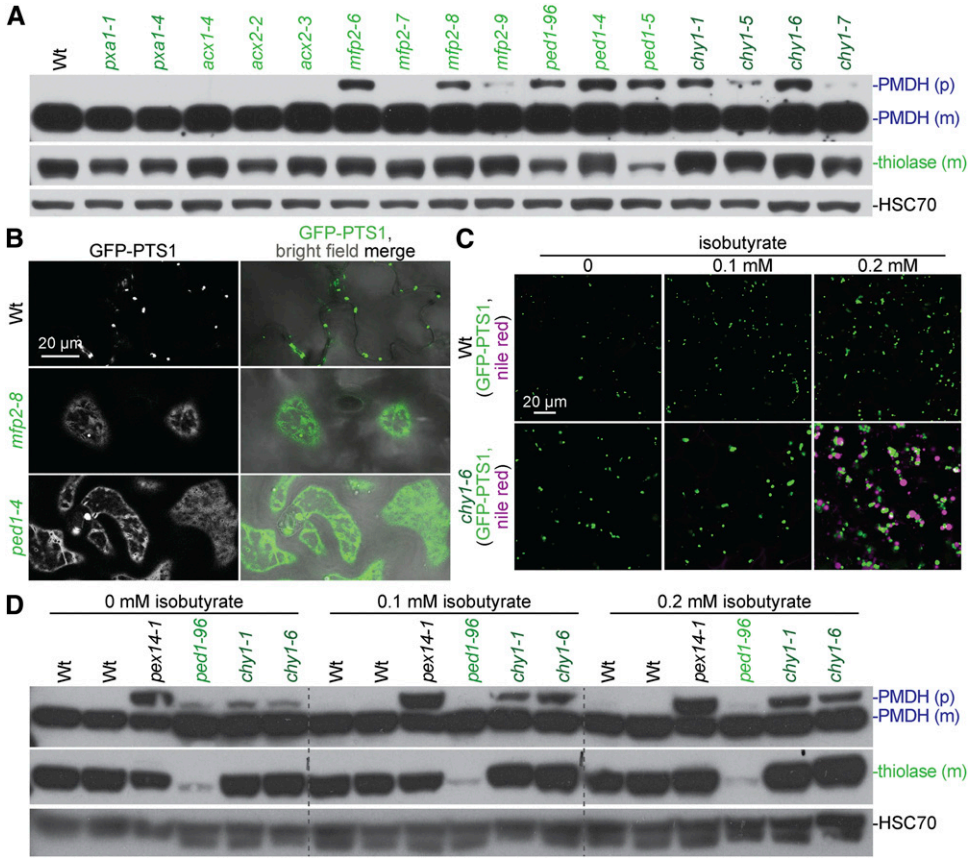

Figure 11 Fatty acid β-oxidation mutants display matrix protein import defects, and *chy1* oil body retention and PTS2-processing defects are worsened by isobutyrate supplementation. (A) Nine-day-old seedlings were prepared for immunoblot analysis and serially probed with antibodies recognizing the indicated proteins. PMDH is translated as a precursor (p) with a PTS2 that is cleaved in the peroxisome to yield mature (m) protein. HSC70 was used as a loading control. (B) Confocal micrographs were taken of 8-day-old cotyledon epidermal cells expressing peroxisomally targeted fluorescence (GFP-PTS1; green). The images used for wild type are the same as those used in Figure 9A. (C) Confocal micrographs were taken of cotyledon epidermal cells of 8-day-old seedlings grown on the indicated concentration of isobutyrate, expressing peroxisomally-targeted fluorescence (GFP-PTS1; white in left panels), and stained with Nile red for oil body visualization (magenta). (D) 8-day-old seedlings grown on the indicated concentration of isobutyrate were prepared for immunoblot analysis and serially probed with antibodies recognizing the indicated proteins. *pex14-1* is a PTS2-processing defective control. Data are representative of two (C) or three (A, B, and D) replicates. Bars, 20 µm.

peroxisomes remained enlarged (Figure 10). This result is consistent with the possibility that peroxisomes become enlarged in *pxn* due to fatty acids accumulating in the peroxisome. Perhaps peroxisomes remain enlarged beyond 5 days because once NAD^+ is depleted, the remaining peroxisomal fatty acids cannot be fully β-oxidized.

To directly test the connection between fatty acid β-oxidation and enlarged *pxn* GFP-PTS1 puncta, we impaired fatty acid import in a *pxn* mutant by crossing to *pxa1-1*. GFP-PTS1 puncta in *pxa1-1 pxn-4* resembled peroxisomes in *pxa1-1* and wild type instead of the large GFP-PTS1 puncta present in *pxn-4* (Figure 13B; Table 2). This epistasis suggests that import of PXA1 substrates into peroxisomes is necessary to produce the large GFP-PTS1 puncta observed in *pxn*, and further supports a requirement for fatty acid import for peroxisome enlargement in fatty acid β-oxidation mutants.

In addition, we crossed *pxn-4* to *ped1-96*. Both mutants displayed enlarged GFP-PTS1 puncta (Figure 13B); *pxn-4* GFP-PTS1 puncta were more enlarged than *ped1-96* puncta (Figure 13B). *pxn-4 ped1-96* GFP-PTS1 puncta resembled *ped1-96*, indicating that removing thiolase activity prevents the extreme enlargement of GFP-PTS1 puncta in *pxn-4* (Figure 13B). Surprisingly, *pxn-4* appeared to enhance the peroxisomal protein import defects of *ped1-96*; both GFP-PTS1 mislocalization to the cytosol and PTS2-processing defects were exacerbated by *pxn-4* (Figure 13, B and D). Given that *ped1-96* import defects likely stem from deficient fatty acid β-oxidation, this result suggests that *pxn* enhances *ped1* defects by further impairing fatty acid β-oxidation, presumably because NAD^+ become limiting inside the peroxisome. Thus, PXN-dependent cofactor import may contribute to peroxisomal β-oxidation.

Mutations in PECTIN METHYLESTERASE31 lead to defects in oil body mobilization

Pectin methylesterases (PME proteins) regulate cell wall structure. Surprisingly, we isolated three independent lines with clustered peroxisomes and mutations in *PECTIN METHYLESTERASE31* (*PME31*): *pme31-1* (R79), *pme31-2* (R363), and *pme31-3* (R922). Whole-genome sequencing of *pme31-1* revealed four homozygous mutations, all on chromosome 3 (Figure 14B, Table S5, and File S1), including a *PME31* mutation that changed Gly141 to Asp (Figure 14A). Recombination mapping using markers for three of the mutations revealed by whole-genome sequencing (Table S6) indicated closer linkage for *pme31-1* than for two other mutations (Figure 14B). Recombination mapping of *pme31-2* indicated linkage at chromosome 3 (Figure 14A), and whole-genome sequencing revealed seven homozygous mutations, all on chromosome 3 (Figure 14B, Table S5, and File S1), including a *PME31* mutation that modified Gly61 to Glu (Figure 14A). Recombination mapping using markers for the mutations revealed by whole-genome

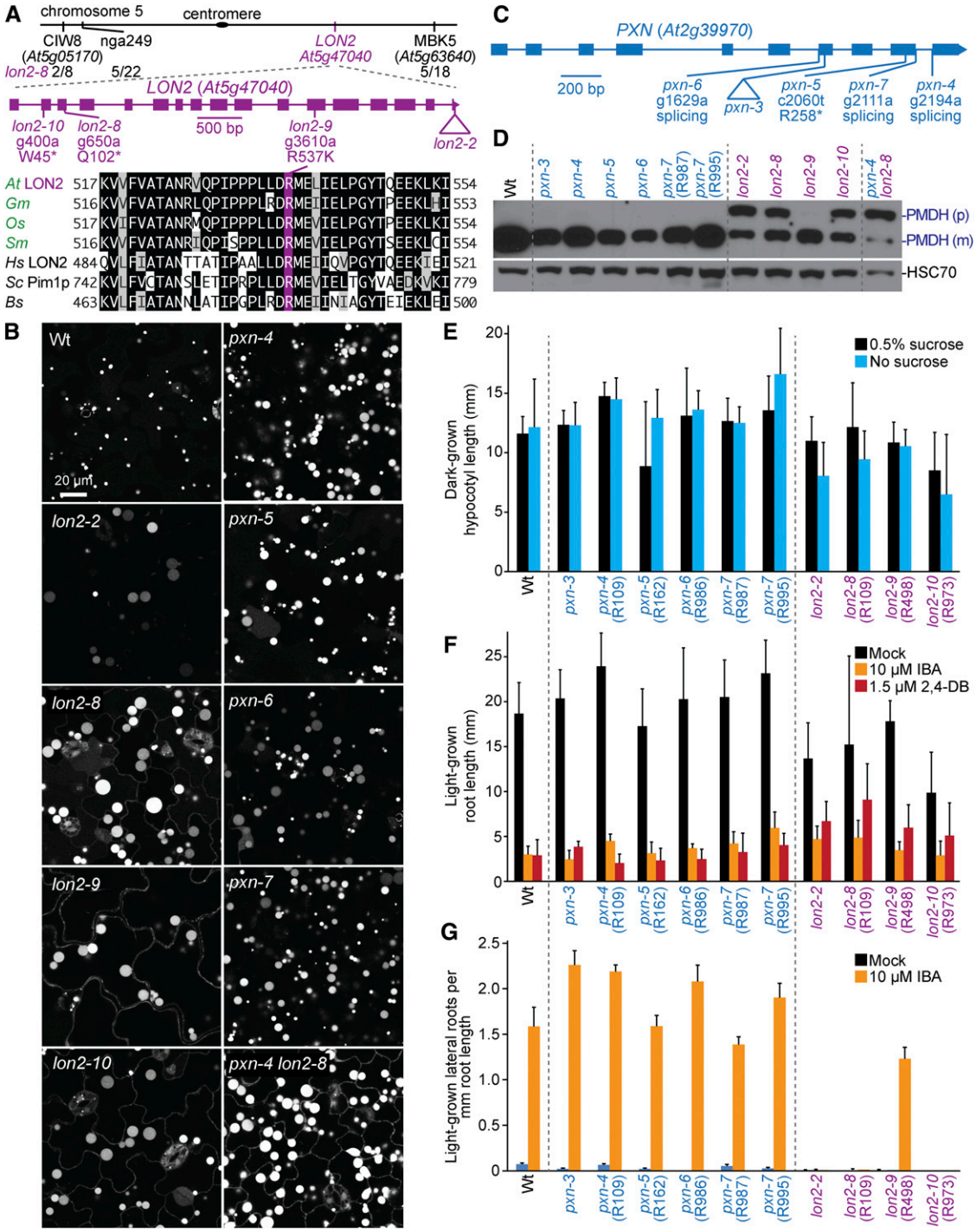

Figure 12 Mutations in *LON2* and *PXN* lead to enlarged GFP-PTS1 puncta, and a subset of *lon2* mutants display GFP-PTS1 mislocalization to the cytosol, PTS2-processing defects, and IBA resistance in lateral root production. (A) Chromosome map indicates the positions of markers used to map *lon2-8* and ratio of recombinants to the number of chromosomes assessed. A gene diagram indicates the positions of *lon2* mutations. LON2 was aligned with related proteins (Table S4); residues are shaded when identical (black or purple) or chemically similar (gray) in at least four sequences. (B) Confocal micrographs were taken of cotyledon epidermal cells of 8-day-old seedlings expressing peroxisomally targeted fluorescence (GFP-PTS1; white). (C) A gene diagram indicates the positions of *pxn* mutations. (D) Eight-day-old seedlings were prepared for immunoblot analysis and serially probed with antibodies recognizing the indicated proteins. PMDH is translated as a precursor (p) with a PTS2 that is cleaved in the peroxisome to yield mature (m) protein. HSC70 was used as a loading control. (E) Hypocotyl lengths of 5-day-old dark-grown seedlings were measured. Error bars show SD ($n \geq 15$). (F) Root lengths of 8-day-old light-grown seedlings were measured. Error bars show SD ($n \geq 17$). (G) Seedlings were grown in the absence of hormone for 4 days and then transferred to either media without hormone or supplemented with IBA for an additional 4 days. The number of lateral roots and root lengths were measured, and the ratio is shown. Error bars show SD ($n = 20$). Data are representative of two (B, D, E, and G) or three (F) replicates. Bar, 20 µm.

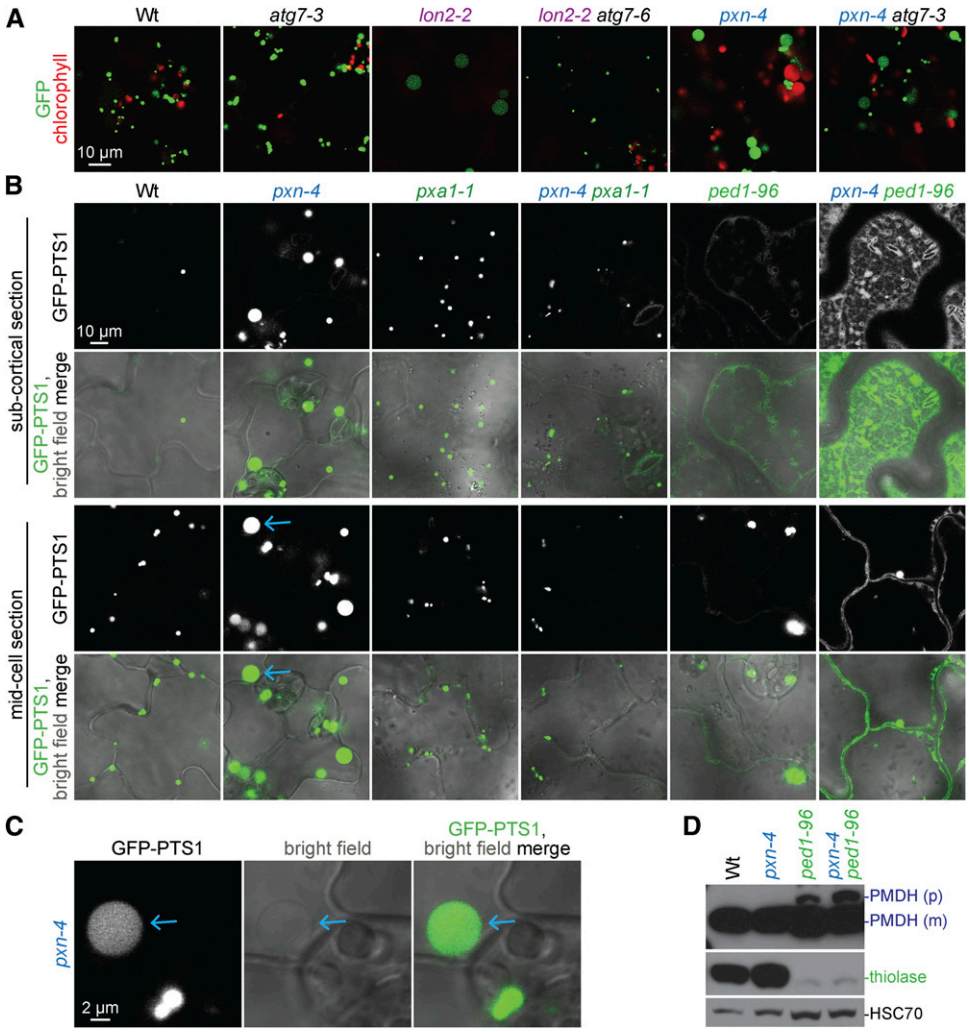

Figure 13 Preventing fatty acid import but not preventing autophagy rescues *pxn* enlarged GFP-PTS1 puncta, and combining *pxn* with *ped1* rescues enlarged GFP-PTS1 puncta while enhancing *ped1* matrix protein import defects. (A) Confocal micrographs were taken of cotyledon epidermal cells of 8-day-old seedlings expressing peroxisomally-targeted fluorescence (GFP-PTS1 in all lines except *lon2-2 atg7-6*, which carried PTS2-GFP; green), and displaying chlorophyll autofluorescence (red). (B) Confocal micrographs were taken of cotyledon epidermal cells of 8-day-old seedlings expressing peroxisomally targeted fluorescence (GFP-PTS1; white in top rows, green in merged images). Blue arrows point to enlarged GFP-PTS1 puncta in *pxn-4* that can be seen in bright field. (C) Digitally enlarged sections of confocal micrographs shown in (B). Blue arrows point to enlarged GFP-PTS1 puncta in *pxn-4* that can be seen in bright field. (D) Eight-day-old seedlings were prepared for immunoblot analysis and serially probed with antibodies recognizing the indicated proteins. PMDH is translated as a precursor (p) with a PTS2 that is cleaved to yield mature (m) protein in the peroxisome. HSC70 was used as a loading control. Data are representative of three replicates (B, D). Bars (A, B), 10 µm; (C), 2 µm.

sequencing (Table S6) indicated close linkage to *pme31-2* (Figure 14B). Whole-genome sequencing of *pme31-3* (Figure 14B, Table S5, and File S1) revealed a *PME31* mutation that changed Gly201 to Asp (Figure 14A). These three altered Gly residues at positions 61, 141, and 201 are conserved in *Arabidopsis* PME proteins (Figure 15A; Dedeurwaerder *et al.* 2009) and in various PME31-related proteins of plants and bacteria (Figure 15A). Although *pme31* mutants were sucrose independent (Figure 14D) and IBA and 2,4-DB sensitive (Figure 14E), they displayed clustered peroxisomes around persisting oil bodies at 4 days (Figure 14C). This phenotype is similar to the one observed for *sdp1*, *pmdh1*, *acx1*, *acx2*, *mfp2*, and *icl* mutants (Figure 2), suggesting that PME31 contributes to lipid mobilization.

Discussion

Seedling peroxisomes cluster around oil bodies

Screening for mutants with altered GFP-PTS1 fluorescence patterns in *Arabidopsis* seedlings revealed numerous mutants displaying clustered peroxisomes around retained oil bodies (Figure 2 and Table S7) with mutations in genes directly or indirectly implicated in lipid mobilization. We presumably isolated these mutants because delayed lipid mobilization led to peroxisomes clustering around retained oil bodies. Peroxisome association with oil bodies reduces distance and increases interaction surfaces between the organelles, thereby increasing the efficiency of lipid mobilization. The SDP1 lipase associates both with the cytosolic side of the peroxisomal membrane and with oil bodies (Eastmond 2006; Thazar-Poulot *et al.* 2015), probably making the released fatty acids more readily available for peroxisomal import. Sucrose supplementation reduces peroxisome–oil body association (Cui *et al.* 2016), suggesting that the close interaction might be favored when the cell needs energy. The importance of peroxisome–oil body interactions is highlighted by the physical proximity we observed in a variety of mutants with impeded lipid mobilization. Peroxisomal β-oxidation of fatty acids stored in oil bodies is important not only in seedlings, but also provides energy for stomatal opening in leaves (McLachlan *et al.* 2016), and it will be interesting to learn whether the mutants isolated here display impairments in stomatal opening.

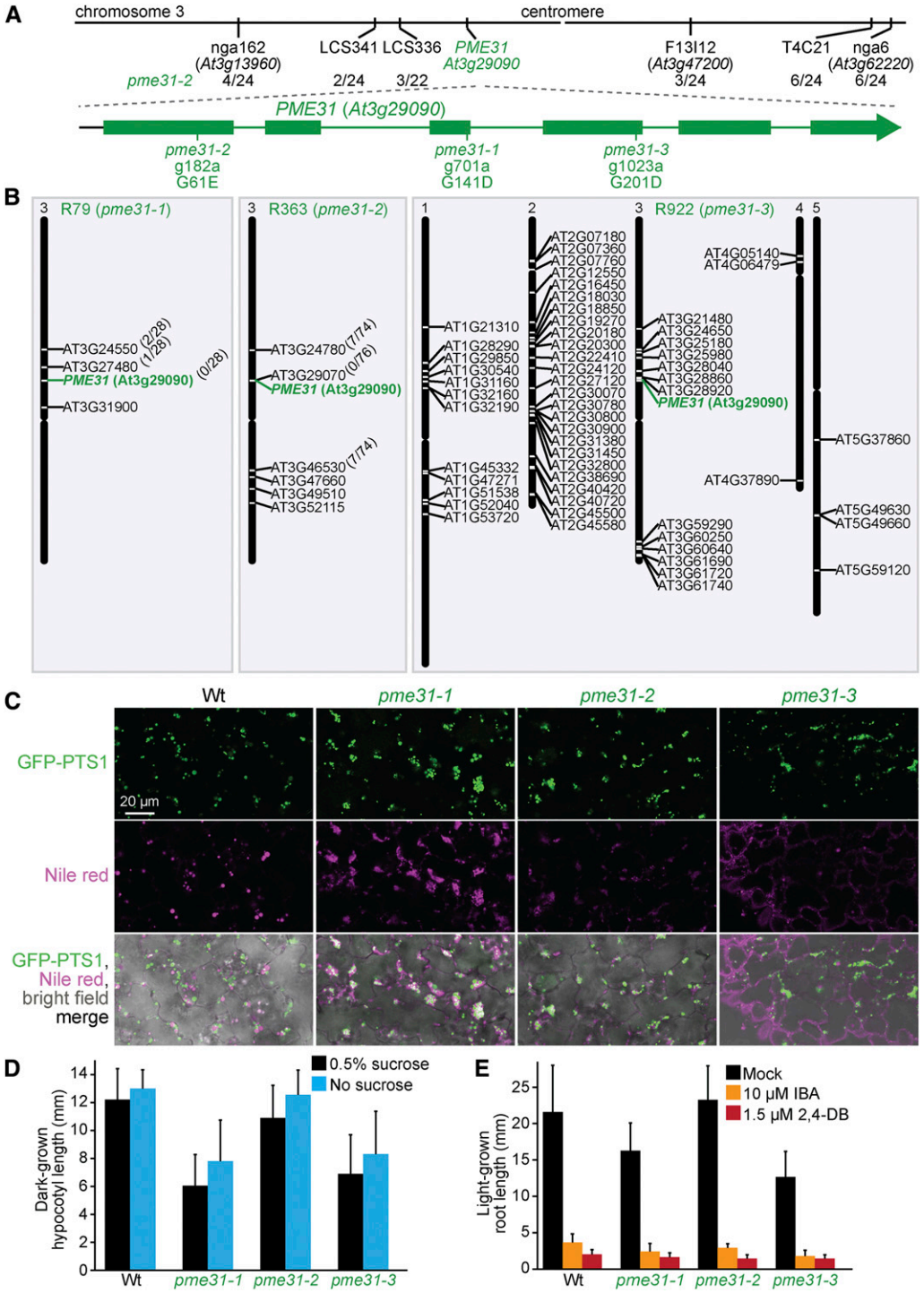

Figure 14 Mutations in *PME31* lead to peroxisome clustering around retained oil bodies. (A) Chromosome map indicates the positions of markers used to map *pme31-2* and ratios of recombinants to the number of chromosomes assessed. A gene diagram indicates the position of *pme31* mutations. (B) Chromosome maps indicate the positions and gene identifier numbers of homozygous EMS-consistent changes in splice sites or nonsynonymous amino acid changes in coding regions. For *pme31-1* and *pme31-2*, genotyping markers for the mutations identified through whole-genome sequencing were used to map in the backcross; the number of recombinants (over the number of chromosomes assessed) are indicated in parentheses. (C) Confocal micrographs were taken of cotyledon epidermal cells of 4-day-old seedlings expressing peroxisomally targeted fluorescence (GFP-PTS1; green) and stained with Nile red for oil body visualization (magenta). (D) Hypocotyl lengths of 5-day-old dark-grown seedlings were measured. Error bars show SD ($n \geq 10$). (E) Root lengths of 8-day-old light-grown seedlings were measured. Error bars show SD ($n = 10$). Data are representative of two replicates (C, E). Bar, 20 µm.

Several mutants, including *sdp1-7*, *pmdh1-2*, *acx1-4*, *acx2-2*, *acx2-3*, *mfp2-7*, *icl-3*, and *icl-4*, displayed clustered peroxisomes (Figure 2 and Table S7) without notable sucrose dependence (Figure 5C, Figure 6D, Figure 7D, and Figure 8D). This finding suggests that microscopic visualization of oil bodies and clustered peroxisomes is more sensitive to impaired β-oxidation than the sucrose dependence phenotype. Most oil bodies are consumed during the first 4 days after germination in wild type (Figure 10; Hayashi *et al.* 1998). By screening 5-day-old seedlings, our screen identified mutants that retained oil bodies (and thus displayed clustered peroxisomes) even slightly longer than wild type. Indeed, this screen was the first forward-genetics screen to isolate mutations in *ACX2*, which is partially redundant with *ACX1*. Although *acx2* mutants are sucrose independent (Figure 6D; Adham *et al.* 2005; Pinfield-Wells *et al.* 2005), *acx2-1* accumulates very long chain fatty acids (Pinfield-Wells *et al.* 2005) because ACX1 and ACX2 have partially distinct

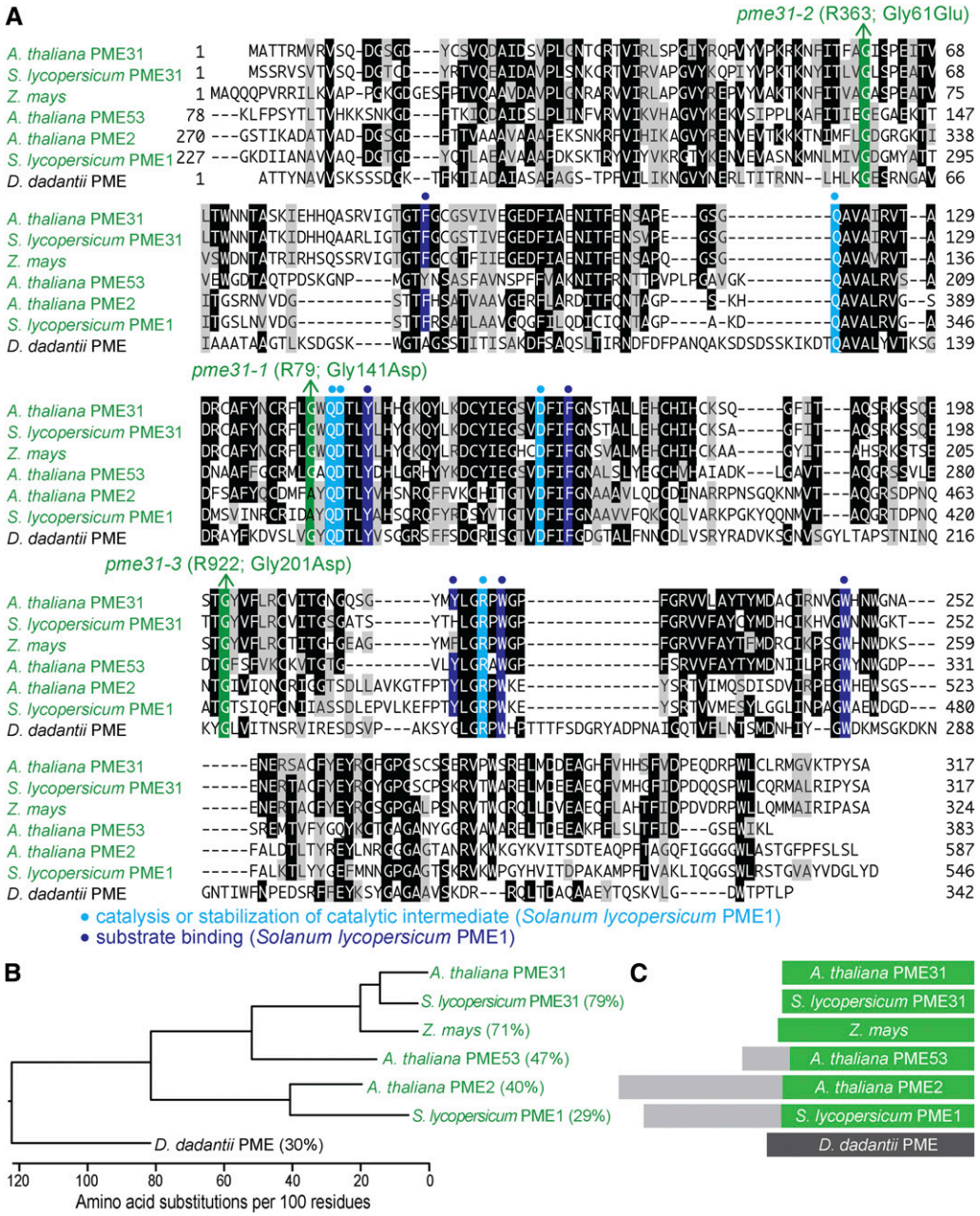

Figure 15 PME31 is closely related to other PME proteins and lacks a predicted signal peptide. (A) PME31 was aligned with related proteins (Table S4); residues are shaded when identical (black or colors) or chemically similar (gray) in at least three sequences. Residues important for catalysis or stabilization of a catalytic intermediate (light blue background and dots) and for substrate binding (dark blue background and dots) in *S. lycopersicum* PME1 are indicated. Mutations identified in this work are denoted (green). (B) Phylogenetic tree of PME proteins constructed using ClustalW on Lasergene MegAlign (DNAStar). (C) Diagram of PME proteins, showing sections of the protein that align (green and dark gray) and the N-terminal extensions present only in some PME proteins (light gray) that target these PME enzymes for secretion to the cell wall (Dedeurwaerder *et al.* 2009).

substrate specificities (Hooks *et al.* 1999). *acx1-4*, *acx2-2*, and *acx2-3* each showed clustered peroxisomes and oil body retention (Figure 2), suggesting that reduced β-oxidation of a subset of acyl-CoA substrates is sufficient to cluster peroxisomes around retained oil bodies. Our observation that some mutants with retained oil bodies were sucrose independent indicates that slight reductions in lipid mobilization do not noticeably impede seedling growth, implying that lipids are normally mobilized faster than necessary to support wild-type growth.

A role for PME31 in lipid mobilization

We were surprised to identify *pme31* mutants in a screen for altered peroxisome positioning. Although PME31 has pectin methylesterase activity *in vitro* (Dedeurwaerder *et al.* 2009), PME31 lacks a signal peptide to direct it to the secretory pathway (Figure 15C) for access to the pectin in the cell wall; PME31 is instead predicted to be cytosolic (Dedeurwaerder *et al.* 2009). In this work we report the first mutations in *PME31*.

We found that mutations in *PME31* led to oil body retention (Figure 14C), much like mutants deficient in lipid mobilization (Figure 2). Because PME31 is predicted to be cytosolic (Dedeurwaerder *et al.* 2009), it is tempting to speculate that PME31 might act as a lipase or otherwise aid in postgerminative lipid mobilization through esterase activity. SDP1 and SDP1L together are responsible for most TAG lipase activity in seedlings, but are less active on diacylglycerol and inactive on monoacylglycerol (Eastmond 2006; Kelly

et al. 2011); the lipase responsible for these activities is not known. It would be interesting to examine PME31 activity on TAG, diacylglycerol, and monoacylglycerol. Moreover, the subcellular localization and protein interaction partners of PME31 in germinating seedlings might provide evidence for direct *vs.* indirect roles for PME31 in β-oxidation. Regardless of the specific role played by PME31 in lipid mobilization, the presence of PME31 homologs that also lack secretion signals (Figure 15) suggests that this role might be conserved in a variety of plants.

Fatty acid β-oxidation influences peroxisome morphology and function

Peroxisome enlargement due to fatty acid β-oxidation defects is a conserved phenomenon. Defects in acyl-CoA oxidase or homologs of the MFP2 multifunctional protein lead to enlarged peroxisomes in yeast (Smith *et al.* 2000; van Roermund 2000) and mammalian cells (Goldfischer *et al.* 1986; Poll-The *et al.* 1988). Similarly, *Arabidopsis mfp2* and *ped1* single mutants and *acx1 acx2* double mutants have enlarged peroxisomes (Figure 9, C–E; Hayashi *et al.* 1998; Germain *et al.* 2001; Pinfield-Wells *et al.* 2005; Rylott *et al.* 2006). GFP-PTS1 puncta were enlarged in *acx2* single mutants (Figure 9D) even though *acx2* mutants lack other notable phenotypes except slightly increased fatty acyl-CoA levels (Pinfield-Wells *et al.* 2005), indicating that peroxisome enlargement can occur when only a subset of fatty acids is inefficiently β-oxidized.

Peroxisomes also become enlarged during the first days of development in wild-type *Arabidopsis* (Figure 10; Mano *et al.* 2002) and cotton (Kunce *et al.* 1984), which is also an oilseed plant. Intense lipid mobilization immediately following germination might saturate the β-oxidation pathway so that fatty acids or β-oxidation intermediates accumulate in peroxisomes. Indeed, supplementation with non-β-oxidizable fatty acids increases peroxisome size in rat hepatocytes (Berge *et al.* 1989; Kryvi *et al.* 1990; Froyland *et al.* 1996).

Fatty acid β-oxidation mutants displayed peroxisomal matrix protein import defects, indicated by partial GFP-PTS1 mislocalization to the cytosol (Figure 9 and Figure 11B), and a defect in removing the PTS2 region from PMDH (Figure 11A). Import defects in fatty acid β-oxidation mutants are also observed in mice; mutations in acyl-CoA oxidase lead to a lack of detectable peroxisomes in some mouse hepatocytes and catalase mislocalization to the cytosol (Fan *et al.* 1996).

Free fatty acids are toxic (Ho *et al.* 1995) and their accumulation in peroxisomes might damage enzymes or cofactors, causing size deregulation and matrix protein import defects. In humans, peroxisome biogenesis disorders can manifest when single enzymes in fatty acid β-oxidation are mutated, perhaps due to very long chain fatty acid accumulation (Waterham *et al.* 2015). Also, fatty acids accumulate in membranes, increasing membrane microviscosity in patients with peroxisome biogenesis disorders (Knazek *et al.* 1983; Whitcomb *et al.* 1988). Peroxisomal membrane fluidity might promote movement of membrane proteins and modulate the frequency of interactions of peroxisomal membrane proteins or complexes, such as the import and export peroxins (Fan *et al.* 1996). *pxn* mutants do not display noticeable matrix protein import defects despite displaying enlarged peroxisomes (Figure 12, B and D; Mano *et al.* 2011), contradicting a previous hypothesis that peroxisome enlargement might confer other defects by reducing the surface-to-volume ratio (De Craemer *et al.* 1991). However, it remains possible that reducing the surface-to-volume ratio might enhance previously existing defects.

Some developmental defects observed in β-oxidation mutants can be explained by reduced β-oxidation of plant hormone precursors. Mutations in fatty acid β-oxidation enzymes can confer IBA resistance (Figure 6E and Figure 7E; Adham *et al.* 2005; Lingard and Bartel 2009; Burkhart *et al.* 2013) and additional defects stemming from reduced auxin levels (Strader *et al.* 2011). β-oxidation also converts the precursor 12-oxo-phytodienoic acid into the plant hormone jasmonic acid. Some developmental defects in fatty acid β-oxidation mutants, such as abnormal inflorescences and flowers and reduced fertility may be caused by reduced jasmonate levels (Richmond and Bleecker 1999; Stintzi and Browse 2000; Delker *et al.* 2007; Schilmiller *et al.* 2007; Castillo and Leon 2008). However, additional defects in fatty acid β-oxidation mutants are not fully explained by loss of known β-oxidation products. For example, *AIM1* and *MFP2* are redundantly required for embryo development (Rylott *et al.* 2006), as are several ACX enzymes (Rylott *et al.* 2003; Khan *et al.* 2012). *PED1* contributes to vegetative growth and floral development (Footitt *et al.* 2007). Defects in ACX proteins and PED1 lead to germination defects that are not rescued by provision of a fixed carbon source (Pinfield-Wells *et al.* 2005). Perhaps the matrix protein import defects observed in this work contribute to these additional developmental defects.

Peroxisome enlargement in pxn is prevented by impeding peroxisomal import of fatty acids

PXN is a transporter implicated in NAD^+ (Agrimi *et al.* 2012; Bernhardt *et al.* 2012; van Roermund *et al.* 2016) and perhaps CoA (Agrimi *et al.* 2012) import into *Arabidopsis* peroxisomes. *pxn* mutants accumulate longer chain fatty acids and display minor oil body retention (Bernhardt *et al.* 2012) but are not sucrose dependent (Figure 12E), suggesting that *pxn* peroxisomes have sufficient cofactors to sustain enough fatty acid β-oxidation for growth immediately following germination. Indeed, our observation that weak mutants in fatty acid β-oxidation displayed oil body retention but not sucrose dependence also supports the conclusion that fatty acid β-oxidation happens at a higher rate than needed for normal seedling growth. It has been postulated that *pxn* β-oxidation defects are mild because seedling peroxisomes synthesized *de novo* from the ER come preloaded with NAD^+ (Bernhardt *et al.* 2012).

In spite of minor physiological defects, *pxn* mutants show striking deregulation of peroxisome size (Figure 10 and

Figure 12B; Mano *et al.* 2004). Although NAD^+ recycling by PMDH within the peroxisome might compensate for reduced import, NAD^+ might be sensitive to destruction by ROS (Antonenkov and Hiltunen 2012) and need to be replaced via PXN import. This necessity would be heightened following the first few days of development when the high rate of fatty acid β-oxidation generates more H_2O_2. Indeed, we found that decreasing fatty acid import by combining *pxn* with *pxa1* fully rescued the enlarged peroxisome phenotype (Figure 13B). Because mutating *PXA1* prevents H_2O_2 production from fatty acid β-oxidation (Eastmond 2007), the rescue of *pxn* peroxisome size by *pxa1* indicates that fatty acid import, and perhaps H_2O_2 accumulation, exacerbates *pxn* defects.

We also examined a double mutant defective in PXN and PED1 and observed peroxisomes the size of *ped1* peroxisomes (Figure 13B), again indicating fatty acid β-oxidation is needed to fully enlarge *pxn* peroxisomes. Interestingly, *pxn* worsened the matrix protein import defects of *ped1-96* (Figure 13, B and D), suggesting that reduced NAD^+ availability further impairs fatty acid β-oxidation and contributes to secondary defects. In contrast, blocking autophagy did not rescue the large peroxisome phenotype in *pxn-4* (Figure 13A), suggesting that *pxn* peroxisomes are enlarged in an autophagy-independent mechanism.

Multiple functions for LON2

LON2 is a peroxisomal protease that is needed for peroxisome maintenance during seedling development (Lingard and Bartel 2009); peroxisomes are degraded via pexophagy when LON2 is dysfunctional (Farmer *et al.* 2013; Goto-Yamada *et al.* 2014). We isolated two *lon2* nonsense alleles and one missense mutation. The *lon2-9* missense allele displayed only a subset of phenotypes similar to null *lon2* mutants whereas other phenotypes were milder (Figure 12). The altered Arg537 residue in *lon2-9* is in the conserved arginine finger that is important for ATPase function in AAA^+ proteins (Besche *et al.* 2004; Iyer *et al.* 2004; Snider and Houry 2008; Cha *et al.* 2010). The distinct phenotypes of *lon2-9* suggest that the arginine finger is not essential for all LON2 functions. Perhaps the lon2-9 protein retains partial function because the AAA^+ domain promotes normal peroxisome morphology but has a smaller role in other LON2 functions. This result agrees with previous findings that the AAA^+ domain is needed for a function related to the microscopic phenotypes, whereas the protease domain is important for peroxisomal protein degradation (Goto-Yamada *et al.* 2014). The subset of defects displayed by *lon2-9* further supports the notion that LON2 has multiple functions.

Distinct cofactor requirements for IBA-to-IAA conversion and fatty acid β- oxidation

PMDH1 and PMDH2 recycle NAD^+ in the peroxisome (Pracharoenwattana *et al.* 2007). Interestingly, *pmdh1* mutants and the *pmdh1-1 pmdh2-1* double mutant were resistant to 2,4-DB but sensitive to IBA (Figure 5D). This result suggests that IBA-to-IAA conversion may be less dependent on NAD^+ than fatty acid or 2,4-DB β-oxidation. In fatty acid β-oxidation, the MFP2 dehydrogenase step uses NAD^+ (Figure 1). Our *mfp2* mutants and previously characterized *mfp2* mutants do not show strong IBA resistance (Figure 7E; Rylott *et al.* 2006). Instead, the dehydrogenase step of IBA β-oxidation might be catalyzed by IBR1, which contains a Rossmann fold that might bind NAD^+, $NADP^+$, or FAD (Zolman *et al.* 2008). The specific cofactor requirements of IBR1 have not been reported.

Conclusions

In summary, this microscopy-based screen recovered a suite of mutants providing insight into peroxisomal pathways. Our screen underscored the connection between peroxisome position (near oil bodies) and function (fatty acid β-oxidation) during seedling establishment. We detected matrix protein import defects in a subset of fatty acid β-oxidation mutants. Because many of the mutants delayed but did not eliminate lipid mobilization, many would not have been recovered had we screened earlier or later in development. Indeed, a previous screen for aberrant peroxisome morphology recovered *drp3a* (Mano *et al.* 2004), *lon2* (Goto-Yamada *et al.* 2014), and *pxn* (Mano *et al.* 2011) alleles, which we also found, but did not report the metabolic mutants that made up the bulk of our isolates.

The depth of screening allowed recovery of multiple mutations in 10 of the 15 genes uncovered (Table 1), including mutants defective in the major seedling isoforms of most enzymes implicated in seedling fatty acid mobilization (Figure 1), mutants in a gene not previously implicated in oil body mobilization (*PME31*), and mutants not previously recovered in forward-genetic screens (*acx2*). We recovered not only null alleles but also partial loss-of-function alleles (*ped1-4*, *icl-3*, *icl-4*, and *lon2-9*) that confer phenotypes distinct from the corresponding null alleles and may aid in future structure-function analyses. This mutant collection will provide useful tools to address nuanced questions about peroxisomal processes in the future.

Acknowledgments

We thank Steven Smith (University of Western Australia) for *pmdh1-1 pmdh1-2* seeds and the PMDH2 antibody, Ian Graham (University of York) for *icl-1* seeds, Pierce Young for the *lon2-9* genotyping marker, and Kim Gonzalez, Yun-Ting Kao, Roxanna Llinas, Andrew Woodward, Zachary Wright, Pierce Young, and an anonymous reviewer for critical comments on the manuscript. This research was supported by the National Science Foundation (MCB-1516966), the National Institutes of Health (NIH) (R01-GM079177), and the Robert A. Welch Foundation (C-1309). Confocal microscopy was performed on equipment obtained through a Shared Instrumentation grant from the NIH (S10-RR026399-01). Whole-genome sequencing at the Genome Technology Access Center at Washington University in St. Louis was supported by the NIH National Center for Research Resources (UL1-RR024992).

Literature Cited

Adham, A. R., B. K. Zolman, A. Millius, and B. Bartel, 2005 Mutations in *Arabidopsis* acyl-CoA oxidase genes reveal distinct and overlapping roles in β-oxidation. Plant J. 41: 859–874.

Agrimi, G., A. Russo, C. L. Pierri, and F. Palmieri, 2012 The peroxisomal NAD+ carrier of *Arabidopsis thaliana* transports coenzyme A and its derivatives. J. Bioenerg. Biomembr. 44: 333–340.

Antonenkov, V. D., and J. K. Hiltunen, 2012 Transfer of metabolites across the peroxisomal membrane. Biochim. Biophys. Acta 1822: 1374–1386.

Arent, S., C. E. Christensen, V. E. Pye, A. Norgaard, and A. Henriksen, 2010 The multifunctional protein in peroxisomal beta-oxidation: structure and substrate specificity of the *Arabidopsis thaliana* protein MFP2. J. Biol. Chem. 285: 24066–24077.

Aung, K., and J. Hu, 2009 The *Arabidopsis* peroxisome division mutant *pdd2* is defective in the *Dynamin-Related Protein3A* (*DRP3A*) gene. Plant Signal. Behav. 4: 542–544.

Bartel, B., L. M. Farmer, M. A. Rinaldi, P. G. Young, C. H. Danan *et al.*, 2014 Mutation of the *Arabidopsis* LON2 peroxisomal protease enhances pexophagy. Autophagy 10: 518–519.

Berge, R. K., A. Aarsland, H. Kryvi, J. Bremer, and N. Aarsaether, 1989 Alkylthioacetic acid (3-thia fatty acids)–a new group of non-beta-oxidizable, peroxisome-inducing fatty acid analogues. I. A study on the structural requirements for proliferation of peroxisomes and mitochondria in rat liver. Biochim. Biophys. Acta 1004: 345–356.

Bernhardt, K., S. Wilkinson, A. P. Weber, and N. Linka, 2012 A peroxisomal carrier delivers NAD(+) and contributes to optimal fatty acid degradation during storage oil mobilization. Plant J. 69: 1–13.

Besche, H., N. Tamura, T. Tamura, and P. Zwickl, 2004 Mutational analysis of conserved AAA+ residues in the archaeal Lon protease from *Thermoplasma acidophilum*. FEBS Lett. 574: 161–166.

Burkhart, S. E., M. J. Lingard, and B. Bartel, 2013 Genetic dissection of peroxisome-associated matrix protein degradation in *Arabidopsis thaliana*. Genetics 193: 125–141.

Burkhart, S. E., Y. T. Kao, and B. Bartel, 2014 Peroxisomal ubiquitin-protein ligases Peroxin2 and Peroxin10 have distinct but synergistic roles in matrix protein import and Peroxin5 retrotranslocation in *Arabidopsis*. Plant Physiol. 166: 1329–1344.

Castillo, M. C., and J. Leon, 2008 Expression of the beta-oxidation gene *3-ketoacyl-CoA thiolase 2* (*KAT2*) is required for the timely onset of natural and dark-induced leaf senescence in *Arabidopsis*. J. Exp. Bot. 59: 2171–2179.

Celenza, J. L., P. L. Grisafi, and G. R. Fink, 1995 A pathway for lateral root formation in *Arabidopsis thaliana*. Genes Dev. 9: 2131–2142.

Cha, S. S., Y. J. An, C. R. Lee, H. S. Lee, Y. G. Kim *et al.*, 2010 Crystal structure of Lon protease: molecular architecture of gated entry to a sequestered degradation chamber. EMBO J. 29: 3520–3530.

Chapman, K. D., J. M. Dyer, and R. T. Mullen, 2012 Biogenesis and functions of lipid droplets in plants: thematic review series: lipid droplet synthesis and metabolism: from yeast to man. J. Lipid Res. 53: 215–226.

Cingolani, P., A. Platts, L. Wang le, M. Coon, T. Nguyen *et al.*, 2012 A program for annotating and predicting the effects of single nucleotide polymorphisms, SnpEff: SNPs in the genome of Drosophila melanogaster strain w1118; iso-2; iso-3. Fly (Austin) 6: 80–92.

Cornah, J. E., V. Germain, J. L. Ward, M. H. Beale, and S. M. Smith, 2004 Lipid utilization, gluconeogenesis, and seedling growth in *Arabidopsis* mutants lacking the glyoxylate cycle enzyme malate synthase. J. Biol. Chem. 279: 42916–42923.

Cui, S., Y. Hayashi, M. Otomo, S. Mano, K. Oikawa *et al.*, 2016 Sucrose production mediated by lipid metabolism suppresses physical interaction of peroxisomes and oil bodies during germination of Arabidopsis thaliana. J. Biol. Chem. DOI: 10.1074/jbc.M116.748814.

De Craemer, D., M. J. Zweens, S. Lyonnet, R. J. Wanders, B. T. Poll-The *et al.*, 1991 Very large peroxisomes in distinct peroxisomal disorders (rhizomelic chondrodysplasia punctata and acyl-CoA oxidase deficiency): novel data. Virchows Arch. A Pathol. Anat. Histopathol. 419: 523–525.

De Marcos Lousa, C., C. W. van Roermund, V. L. Postis, D. Dietrich, I. D. Kerr *et al.*, 2013 Intrinsic acyl-CoA thioesterase activity of a peroxisomal ATP binding cassette transporter is required for transport and metabolism of fatty acids. Proc. Natl. Acad. Sci. USA 110: 1279–1284.

Dedeurwaerder, S., L. Menu-Bouaouiche, A. Mareck, P. Lerouge, and F. Guerineau, 2009 Activity of an atypical *Arabidopsis thaliana* pectin methylesterase. Planta 229: 311–321.

Delker, C., B. K. Zolman, O. Miersch, and C. Wasternack, 2007 Jasmonate biosynthesis in *Arabidopsis thaliana* requires peroxisomal beta-oxidation enzymes–additional proof by properties of *pex6* and *aim1*. Phytochemistry 68: 1642–1650.

Dietrich, D., H. Schmuths, C. De Marcos Lousa, J. M. Baldwin, S. A. Baldwin *et al.*, 2009 Mutations in the *Arabidopsis* peroxisomal ABC transporter COMATOSE allow differentiation between multiple functions in planta: insights from an allelic series. Mol. Biol. Cell 20: 530–543.

Eastmond, P. J., 2006 *Sugar-dependent1* encodes a patatin domain triacylglycerol lipase that initiates storage oil breakdown in germinating *Arabidopsis* seeds. Plant Cell 18: 665–675.

Eastmond, P. J., 2007 *Monodehyroascorbate reductase 4* is required for seed storage oil hydrolysis and postgerminative growth in *Arabidopsis*. Plant Cell 19: 1376–1387.

Eastmond, P. J., V. Germain, P. R. Lange, J. H. Bryce, S. M. Smith *et al.*, 2000a Postgerminative growth and lipid catabolism in oilseeds lacking the glyoxylate cycle. Proc. Natl. Acad. Sci. USA 97: 5669–5674.

Eastmond, P. J., M. Hooks, and I. A. Graham, 2000b The *Arabidopsis* acyl-CoA oxidase gene family. Biochem. Soc. Trans. 28: 95–99.

Enders, T. A., and L. C. Strader, 2015 Auxin activity: past, present, and future. Am. J. Bot. 102: 180–196.

Fan, C. Y., J. Pan, R. Chu, D. Lee, K. D. Kluckman *et al.*, 1996 Hepatocellular and hepatic peroxisomal alterations in mice with a disrupted peroxisomal fatty acyl-coenzyme A oxidase gene. J. Biol. Chem. 271: 24698–24710.

Farmer, L. M., M. A. Rinaldi, P. G. Young, C. H. Danan, S. E. Burkhart *et al.*, 2013 Disrupting autophagy restores peroxisome function to an *Arabidopsis lon2* mutant and reveals a role for the LON2 protease in peroxisomal matrix protein degradation. Plant Cell 25: 4085–4100.

Footitt, S., S. P. Slocombe, V. Larner, S. Kurup, Y. Wu *et al.*, 2002 Control of germination and lipid mobilization by *COMATOSE*, the *Arabidopsis* homologue of human ALDP. EMBO J. 21: 2912–2922.

Footitt, S., J. E. Cornah, I. Pracharoenwattana, J. H. Bryce, and S. M. Smith, 2007 The *Arabidopsis 3-ketoacyl-CoA thiolase-2* (*kat2–1*) mutant exhibits increased flowering but reduced reproductive success. J. Exp. Bot. 58: 2959–2968.

Froyland, L., K. Helland, G. K. Totland, H. Kryvi, and R. K. Berge, 1996 A hypolipidemic peroxisome proliferating fatty acid induces polydispersity of rat liver mitochondria. Biol. Cell 87: 105–112.

Fujimoto, M., S. Arimura, S. Mano, M. Kondo, C. Saito *et al.*, 2009 *Arabidopsis* dynamin-related proteins DRP3A and DRP3B are functionally redundant in mitochondrial fission, but have distinct roles in peroxisomal fission. Plant J. 58: 388–400.

Fulda, M., J. Shockey, M. Werber, F. P. Wolter, and E. Heinz, 2002 Two long-chain acyl-CoA synthetases from *Arabidopsis thaliana* involved in peroxisomal fatty acid β-oxidation. Plant J. 32: 93–103.

Fulda, M., J. Schnurr, A. Abbadi, E. Heinz, and J. Browse, 2004 Peroxisomal acyl-CoA synthetase activity is essential for seedling development in *Arabidopsis thaliana*. Plant Cell 16: 394–405.

Gabaldon, T., 2010 Peroxisome diversity and evolution. Philos. Trans. R. Soc. Lond. B Biol. Sci. 365: 765–773.

Germain, V., E. L. Rylott, T. R. Larson, S. M. Sherson, N. Bechntold *et al.*, 2001 Requirement for 3-ketoacyl-CoA thiolase-2 in peroxisome development, fatty acid β-oxidation and breakdown of triacylglycerol in lipid bodies of *Arabidopsis* seedlings. Plant J. 28: 1–12.

Goldfischer, S., J. Collins, I. Rapin, P. Neumann, W. Neglia *et al.*, 1986 Pseudo-Zellweger syndrome: deficiencies in several peroxisomal oxidative activities. J. Pediatr. 108: 25–32.

Goto, S., S. Mano, C. Nakamori, and M. Nishimura, 2011 *Arabidopsis* aberrant peroxisome morphology9 is a peroxin that recruits the PEX1–PEX6 complex to peroxisomes. Plant Cell 23: 1573–1587.

Goto-Yamada, S., S. Mano, C. Nakamori, M. Kondo, R. Yamawaki *et al.*, 2014 Chaperone and protease functions of LON protease 2 modulate the peroxisomal transition and degradation with autophagy. Plant Cell Physiol. 55: 482–496.

Gould, S. J., G. A. Keller, N. Hosken, J. Wilkinson, and S. Subramani, 1989 A conserved tripeptide sorts proteins to peroxisomes. J. Cell Biol. 108: 1657–1664.

Graham, I. A., 2008 Seed storage oil mobilization. Annu. Rev. Plant Biol. 59: 115–142.

Graham, I. A., Y. Li, and T. R. Larson, 2002 Acyl-CoA measurements in plants suggest a role in regulating various cellular processes. Biochem. Soc. Trans. 30: 1095–1099.

Hamada, T., H. Igarashi, M. Yao, T. Hashimoto, T. Shimmen *et al.*, 2006 Purification and characterization of plant dynamin from tobacco BY-2 cells. Plant Cell Physiol. 47: 1175–1181.

Haughn, G. W., and C. Somerville, 1986 Sulfonylurea-resistant mutants of *Arabidopsis thaliana*. Mol. Gen. Genet. 204: 430–434.

Hayashi, H., K. Nito, R. Takei-Hoshi, M. Yagi, M. Kondo *et al.*, 2002 Ped3p is a peroxisomal ATP-binding cassette transporter that might supply substrates for fatty acid β-oxidation. Plant Cell Physiol. 43: 1–11.

Hayashi, M., K. Toriyama, M. Kondo, and M. Nishimura, 1998 2,4-dichlorophenoxybutyric acid-resistant mutants of *Arabidopsis* have defects in glyoxysomal fatty acid β-oxidation. Plant Cell 10: 183–195.

Helm, M., C. Luck, J. Prestele, G. Hierl, P. F. Huesgen *et al.*, 2007 Dual specificities of the glyoxysomal/peroxisomal processing protease Deg15 in higher plants. Proc. Natl. Acad. Sci. USA 104: 11501–11506.

Ho, J. K., H. Moser, Y. Kishimoto, and J. A. Hamilton, 1995 Interactions of a very long chain fatty acid with model membranes and serum albumin. Implications for the pathogenesis of adrenoleukodystrophy. J. Clin. Invest. 96: 1455–1463.

Hooks, M. A., F. Kellas, and I. A. Graham, 1999 Long-chain acyl-CoA oxidases of *Arabidopsis*. Plant J. 20: 1–13.

Hu, J., A. Baker, B. Bartel, N. Linka, R. T. Mullen *et al.*, 2012 Plant peroxisomes: biogenesis and function. Plant Cell 24: 2279–2303.

Iyer, L. M., D. D. Leipe, E. V. Koonin, and L. Aravind, 2004 Evolutionary history and higher order classification of AAA+ ATPases. J. Struct. Biol. 146: 11–31.

Kelly, A. A., A. L. Quettier, E. Shaw, and P. J. Eastmond, 2011 Seed storage oil mobilization is important but not essential for germination or seedling establishment in *Arabidopsis*. Plant Physiol. 157: 866–875.

Khan, B. R., A. R. Adham, and B. K. Zolman, 2012 Peroxisomal Acyl-CoA oxidase 4 activity differs between *Arabidopsis* accessions. Plant Mol. Biol. 78: 45–58.

Knazek, R. A., W. B. Rizzo, J. D. Schulman, and J. R. Dave, 1983 Membrane microviscosity is increased in the erythrocytes of patients with adrenoleukodystrophy and adrenomyeloneuropathy. J. Clin. Invest. 72: 245–248.

Kryvi, H., A. Aarsland, and R. K. Berge, 1990 Morphologic effects of sulfur-substituted fatty acids on rat hepatocytes with special reference to proliferation of peroxisomes and mitochondria. J. Struct. Biol. 103: 257–265.

Kunce, C. M., R. N. Trelease, and D. C. Doman, 1984 Ontogeny of glyoxysomes in maturing and germinated cotton seeds-a morphometric analysis. Planta 161: 156–164.

Lachtermacher, M. B., H. N. Seuanez, A. B. Moser, H. W. Moser, and K. D. Smith, 2000 Determination of 30 X-linked adrenoleukodystrophy mutations, including 15 not previously described. Hum. Mutat. 15: 348–353.

Lai, Z., F. Wang, Z. Zheng, B. Fan, and Z. Chen, 2011 A critical role of autophagy in plant resistance to necrotrophic fungal pathogens. Plant J. 66: 953–968.

Lange, P., P. Eastmond, K. Madagan, and I. Graham, 2004 An *Arabidopsis* mutant disrupted in valine catabolism is also compromised in peroxisomal fatty acid beta-oxidation. FEBS Lett. 571: 147–153.

Li, F., and R. D. Vierstra, 2012 Autophagy: a multifaceted intracellular system for bulk and selective recycling. Trends Plant Sci. 17: 526–537.

Li, H., B. Handsaker, A. Wysoker, T. Fennell, J. Ruan *et al.*, 2009 The Sequence Alignment/Map format and SAMtools. Bioinformatics 25: 2078–2079.

Lingard, M. J., and B. Bartel, 2009 *Arabidopsis* LON2 is necessary for peroxisomal function and sustained matrix protein import. Plant Physiol. 151: 1354–1365.

Lingard, M. J., M. Monroe-Augustus, and B. Bartel, 2009 Peroxisome-associated matrix protein degradation in *Arabidopsis*. Proc. Natl. Acad. Sci. USA 106: 4561–4566.

Lucas, K. A., J. R. Filley, J. M. Erb, E. R. Graybill, and J. W. Hawes, 2007 Peroxisomal metabolism of propionic acid and isobutyric acid in plants. J. Biol. Chem. 282: 24980–24989.

Maeshima, M., H. Yokoi, and T. Asahi, 1988 Evidence for no proteolytic processing during transport of isocitrate lyase into glyoxysomes in castor bean endosperm. Plant Cell Physiol. 29: 381–384.

Mano, S., C. Nakamori, M. Hayashi, A. Kato, M. Kondo *et al.*, 2002 Distribution and characterization of peroxisomes in *Arabidopsis* by visualization with GFP: dynamic morphology and actin-dependent movement. Plant Cell Physiol. 43: 331–341.

Mano, S., C. Nakamori, M. Kondo, M. Hayashi, and M. Nishimura, 2004 An *Arabidopsis* dynamin-related protein, DRP3A, controls both peroxisomal and mitochondrial division. Plant J. 38: 487–498.

Mano, S., C. Nakamori, K. Nito, M. Kondo, and M. Nishimura, 2006 The *Arabidopsis pex12* and *pex13* mutants are defective in both PTS1- and PTS2-dependent protein transport to peroxisomes. Plant J. 47: 604–618.

Mano, S., C. Nakamori, Y. Fukao, M. Araki, A. Matsuda *et al.*, 2011 A defect of peroxisomal membrane protein 38 causes enlargement of peroxisomes. Plant Cell Physiol. 52: 2157–2172.

McLachlan, D. H., J. Lan, C. M. Geilfus, A. N. Dodd, T. Larson *et al.*, 2016 The breakdown of stored triacylglycerols is required during light-induced stomatal opening. Curr. Biol. 26: 707–712.

Monroe-Augustus, M., N. M. Ramon, S. E. Ratzel, M. J. Lingard, S. E. Christensen *et al.*, 2011 Matrix proteins are inefficiently imported into *Arabidopsis* peroxisomes lacking the receptor-docking peroxin PEX14. Plant Mol. Biol. 77: 1–15.

Normanly, J., 1997 Auxin metabolism. Physiol. Plant. 100: 431–442.

Olsen, L. J., W. F. Ettinger, B. Damsz, K. Matsudaira, M. A. Webb *et al.*, 1993 Targeting of glyoxysomal proteins to peroxisomes in leaves and roots of a higher plant. Plant Cell 5: 941–952.

Pinfield-Wells, H., E. L. Rylott, A. D. Gilday, S. Graham, K. Job *et al.*, 2005 Sucrose rescues seedling establishment but not germination of *Arabidopsis* mutants disrupted in peroxisomal fatty acid catabolism. Plant J. 43: 861–872.

Poll-The, B. T., F. Roels, H. Ogier, J. Scotto, J. Vamecq *et al.*, 1988 A new peroxisomal disorder with enlarged peroxisomes and a specific deficiency of acyl-CoA oxidase (pseudo-neonatal adrenoleukodystrophy). Am. J. Hum. Genet. 42: 422–434.

Pracharoenwattana, I., J. E. Cornah, and S. M. Smith, 2007 *Arabidopsis* peroxisomal malate dehydrogenase functions in beta-oxidation but not in the glyoxylate cycle. Plant J. 50: 381–390.

Ramón, N. M., and B. Bartel, 2010 Interdependence of the peroxisome-targeting receptors in *Arabidopsis thaliana*: PEX7 facilitates PEX5 accumulation and import of PTS1 cargo into peroxisomes. Mol. Biol. Cell 21: 1263–1271.

Richmond, T. A., and A. B. Bleecker, 1999 A defect in β-oxidation causes abnormal inflorescence development in *Arabidopsis*. Plant Cell 11: 1911–1923.

Russell, L., V. Larner, S. Kurup, S. Bougourd, and M. Holdsworth, 2000 The *Arabidopsis comatose* locus regulates germination potential. Development 127: 3759–3767.

Rylott, E. L., C. A. Rogers, A. D. Gilday, T. Edgell, T. R. Larson *et al.*, 2003 *Arabidopsis* mutants in short- and medium-chain acyl-CoA oxidase activities accumulate acyl-CoAs and reveal that fatty acid β-oxidation is essential for embryo development. J. Biol. Chem. 278: 21370–21377.

Rylott, E. L., P. J. Eastmond, A. D. Gilday, S. P. Slocombe, T. R. Larson *et al.*, 2006 The *Arabidopsis thaliana* multifunctional protein gene (*MFP2*) of peroxisomal beta-oxidation is essential for seedling establishment. Plant J. 45: 930–941.

Schilmiller, A. L., A. J. Koo, and G. A. Howe, 2007 Functional diversification of acyl-coenzyme A oxidases in jasmonic acid biosynthesis and action. Plant Physiol. 143: 812–824.

Shani, N., P. A. Watkins, and D. Valle, 1995 *PXA1*, a possible *Saccharomyces cerevisiae* ortholog of the human adrenoleukodystrophy gene. Proc. Natl. Acad. Sci. USA 92: 6012–6016.

Shani, N., A. Sapag, and D. Valle, 1996 Characterization and analysis of conserved motifs in a peroxisomal ATP-binding cassette transporter. J. Biol. Chem. 271: 8725–8730.

Smith, J. J., T. W. Brown, G. A. Eitzen, and R. A. Rachubinski, 2000 Regulation of peroxisome size and number by fatty acid beta-oxidation in the yeast *Yarrowia lipolytica*. J. Biol. Chem. 275: 20168–20178.

Snider, J., and W. A. Houry, 2008 AAA+ proteins: diversity in function, similarity in structure. Biochem. Soc. Trans. 36: 72–77.

Stasinopoulos, T. C., and R. P. Hangarter, 1990 Preventing photochemistry in culture media by long-pass light filters alters growth of cultured tissues. Plant Physiol. 93: 1365–1369.

Stintzi, A., and J. Browse, 2000 The *Arabidopsis* male-sterile mutant, *opr3*, lacks the 12-oxophytodienoic acid reductase required for jasmonate synthesis. Proc. Natl. Acad. Sci. USA 97: 10625–10630.

Strader, L. C., and B. Bartel, 2011 Transport and metabolism of the endogenous auxin precursor indole-3-butyric acid. Mol. Plant 4: 477–486.

Strader, L. C., D. L. Wheeler, S. E. Christensen, J. C. Berens, J. D. Cohen *et al.*, 2011 Multiple facets of *Arabidopsis* seedling development require indole-3-butyric acid-derived auxin. Plant Cell 23: 984–999.

Swinkels, B. W., S. J. Gould, A. G. Bodnar, R. A. Rachubinski, and S. Subramani, 1991 A novel, cleavable peroxisomal targeting signal at the amino-terminus of the rat 3-ketoacyl-CoA thiolase. EMBO 10: 3255–3262.

Thazar-Poulot, N., M. Miquel, I. Fobis-Loisy, and T. Gaude, 2015 Peroxisome extensions deliver the *Arabidopsis* SDP1 lipase to oil bodies. Proc. Natl. Acad. Sci. USA 112: 4158–4163.

Thole, J. M., and L. C. Strader, 2015 Next-generation sequencing as a tool to quickly identify causative EMS-generated mutations. Plant Signal. Behav. 10: e1000167.

Thole, J. M., E. R. Beisner, J. Liu, S. V. Venkova, and L. C. Strader, 2014 Abscisic acid regulates root elongation through the activities of auxin and ethylene in *Arabidopsis thaliana*. G3 (Bethesda) 4: 1259–1274.

van Roermund, C. W., H. F. Tabak, M. van Den Berg, R. J. Wanders, and E. H. Hettema, 2000 Pex11p plays a primary role in medium-chain fatty acid oxidation, a process that affects peroxisome number and size in *Saccharomyces cerevisiae*. J. Cell Biol. 150: 489–498.

van Roermund, C. W., M. G. Schroers, J. Wiese, F. Facchinelli, S. Kurz *et al.*, 2016 The peroxisomal NAD carrier from *Arabidopsis* imports NAD in exchange with AMP. Plant Physiol. 171: 2127–2139.

Wain, R. L., and F. Wightman, 1954 The growth-regulating activity of certain ω-substituted alkyl carboxylic acids in relation to their β-oxidation within the plant. Proc. R. Soc. Lond. B Biol. Sci. 142: 525–536.

Waterham, H. R., S. Ferdinandusse, and R. J. Wanders, 2016 Human disorders of peroxisome metabolism and biogenesis. Biochim. Biophys. Acta. 1863: 922–933.

Whitcomb, R. W., W. M. Linehan, and R. A. Knazek, 1988 Effects of long-chain, saturated fatty acids on membrane microviscosity and adrenocorticotropin responsiveness of human adrenocortical cells in vitro. J. Clin. Invest. 81: 185–188.

Wichers, M., W. Kohler, W. Brennemann, V. Boese, P. Sokolowski *et al.*, 1999 X-linked adrenomyeloneuropathy associated with 14 novel ALD-gene mutations: no correlation between type of mutation and age of onset. Hum. Genet. 105: 116–119.

Wiszniewski, A. A., J. D. Bussell, R. L. Long, and S. M. Smith, 2014 Knockout of the two evolutionarily conserved peroxisomal 3-ketoacyl-CoA thiolases in *Arabidopsis* recapitulates the *abnormal inflorescence meristem 1* phenotype. J. Exp. Bot. 65: 6723–6733.

Woodward, A. W., and B. Bartel, 2005 Auxin: regulation, action, and interaction. Ann. Bot. (Lond.) 95: 707–735.

Woodward, A. W., W. A. Fleming, S. E. Burkhart, S. E. Ratzel, M. Bjornson *et al.*, 2014 A viable *Arabidopsis pex13* missense allele confers severe peroxisomal defects and decreases PEX5 association with peroxisomes. Plant Mol. Biol. 86: 201–214.

Young, P. G., and B. Bartel, 2016 Pexophagy and peroxisomal protein turnover in plants. Biochim. Biophys. Acta 1863: 999–1005.

Zhang, X., and J. Hu, 2009 Two small protein families, dynamin-related protein3 and fission1, are required for peroxisome fission in *Arabidopsis*. Plant J. 57: 146–159.

Zhang, X., and J. Hu, 2010 The *Arabidopsis* chloroplast division protein dynamin- related protein5b also mediates peroxisome division. Plant Cell 22: 431–442.

Zhang, X. C., and J. P. Hu, 2008 Fission1A and fission1B proteins mediate the fission of peroxisomes and mitochondria in *Arabidopsis*. Mol. Plant 1: 1036–1047.

Zolman, B. K., and B. Bartel, 2004 An *Arabidopsis* indole-3-butyric acid-response mutant defective in peroxin6, an apparent ATPase

implicated in peroxisomal function. Proc. Natl. Acad. Sci. USA 101: 1786–1791.
Zolman, B. K., A. Yoder, and B. Bartel, 2000 Genetic analysis of indole-3-butyric acid responses in *Arabidopsis thaliana* reveals four mutant classes. Genetics 156: 1323–1337.
Zolman, B. K., M. Monroe-Augustus, B. Thompson, J. W. Hawes, K. A. Krukenberg *et al.*, 2001a *chy1*, an *Arabidopsis* mutant with impaired β-oxidation, is defective in a peroxisomal β-hydroxyisobutyryl-CoA hydrolase. J. Biol. Chem. 276: 31037–31046.
Zolman, B. K., I. D. Silva, and B. Bartel, 2001b The *Arabidopsis pxa1* mutant is defective in an ATP-binding cassette transporter-like protein required for peroxisomal fatty acid beta-oxidation. Plant Physiol. 127: 1266–1278.
Zolman, B. K., M. Nyberg, and B. Bartel, 2007 IBR3, a novel peroxisomal acyl-CoA dehydrogenase-like protein required for indole-3-butyric acid response. Plant Mol. Biol. 64: 59–72.
Zolman, B. K., N. Martinez, A. Millius, A. R. Adham, and B. Bartel, 2008 Identification and characterization of *Arabidopsis* indole-3-butyric acid response mutants defective in novel peroxisomal enzymes. Genetics 180: 237–251.

Communicating editor: S. Poethig

Table S1: PCR-based markers used to genotype identified mutants, reference lines, and constructs

Mutant	Alias	Primer name (5' to 3' sequence)	Enzyme	Amplicon size (bp) Wt	Mutant
acx1-4	R574	R574-1 (CCTCTTCCGAATATAACTGTTGGTGATCTC) R574-2 (CCGATGGAACATATTCTCCTTCTCTTG)	*Ava*I	184, 87, 27	211, 87
acx2-2	R223	R233-1 (GTATATATTTGCAGTCTCGG) R737-ACX2-R (CAGTCATGGCAAAGCAACC)	*Ava*I	102, 16	118
acx2-3	R737	ACX2-5 (TAAGATGGGCGTTCAATACAGG) R737-ACX2-R (CAGTCATGGCAAAGCAACC)	*Bsa*XI	162, 30, 74	266
atg7-3	SAIL_11_H07	ATG7-23 (GTTGCCATGTCTAATCCAGTCAGG) ATG7-Tsp45I (GTTGCCATGTCTAATCCAGTCAGG)	-	539	-
		LB1-SAIL (GCCTTTTCAGAAATGGATAAATAGCCTTGCTTCC) ATG7-24 (GTTGCCATGTCTAATCCAGTCAGG)	-	-	~350
chy1-1		K14B20-20 (AGAAGTAATTGGCACCGAGTCTCCAGGTAC) K14B20-21 (ACCCTAGTGTGAAACTTGTCATCCTAAAGG)	*Kpn*I	228	258
chy1-5	R189	R189-1 (AGGTCTCGCTATAATTTCGTTTTG) R189-2 (GGAGGCGCCTACATCTGGA)	*Aci*I	185, 103	288
chy1-6	R499/R506	R499-F (GGATGACAAATAGGTCGC) R499-ApoI-R (CAAGAAGTAGGAGGCGCCTAAAT)	*Apo*I	117	93, 24
chy1-7	R728	R728-1 (TTTCTTGTCTTTTTTGTCCA) R728-2 (CGTTGAAGGCACAAAATGAGTTGC)	*Sty*I	106	88, 18
drp3a-3	SALK_066958	drp3a-3-1 (AACCGCACAGTCAAGGAAGC) drp3a-3-2 (TATCCGCGACTTCAAATCCG)	-	544	-
		drp3a-3-1 (AACCGCACAGTCAAGGAAGC) LB1-SALK (CAAACCAGCGTGGACCGCTTGCTGCAACTC)	-	-	~150
drp3a-4	R224	drp3a-1-1 (TTCCCTTCCTTGCTTTATTTG) drp3a-1-2 (GGGACGCCTATGGTGATG)	*Dra*I	533	333, 200
drp3a-5	R402	R402-1 (CGCCTTCTCCGTCTTCCT) R402-2 (AATCTATTCGTCTCAGCCTACAAA)	*Mlu*I	239, 219	458
icl-3	R291	R291-1 (AAGAAGGGAGATTCGAAGCC) R291-2 (ATGGCCACGTAGAGCCACCACG)	*Sty*I	116	97, 19
icl-4	R601	R601-1 (GTACGGCCTCTCGCACCTTA) R601-2 (TGTGTGAGTGGACGAGCACTGCC)	*Dde*I	93, 17	110
icl-5	R951	R951-1 (TTTCCGTATTATTTGTTAGGTTCC) R951-2 (ATCAGGGCTTGCCGTTTCCATCC)	*Dde*I	316	184, 132
lon2-2	SALK_043857	LON2-17 (TGATTCCTTACCATATGGGCCAACACAGTCC) LON2-16 (AGTCTTGTTCTCGGTATTGCATTGGGGGTAG)	-	350	-
		LON2-17 (TGATTCCTTACCATATGGGCCAACACAGTCC) LB1-SALK (CAAACCAGCGTGGACCGCTTGCTGCAACTC)	-	-	~350
lon2-8	R109	lon2-R109-F (GTGCTGGAAGTGATTCTGG) lon2-R109-R-RsaI (CTGGTGTGCCATTGAAGATCGT)	*Rsa*I	59, 47	47, 36, 23
lon2-9	R498	LON2-HpaII (TCAACCTATTCCACCTCCTCTTCTAGACC) LON2-24 (CCTCCTTCGGCCATTCTACCATTA)	*Hpa*II	258, 147, 28	286, 147
lon2-10	R973	R973-1 (TCAGCGTCACACTAGTGGAGCAAGAGCCAT) R973-2 (GGATTAATCATCGTCCCAATTGAAGAACCC)	*Nco*I	88, 27	115
mdar4-4 (*sdp2-4*)	SALK_068667	sdp2-4-1 (GGGAATGCGGTTGTTATCG) sdp2-4-2 (AGTGGCTCCCGTCTTTGA)	-	537	-
		LB1-SALK (CAAACCAGCGTGGACCGCTTGCTGCAACTC) sdp2-4-2 (AGTGGCTCCCGTCTTTGA)	-	-	~251
mdar4-5	R340/R343	R340-MDAR-4-F (ACTATAAGTTACAAATTCTTGATCATTGCAACGG) R340-MDAR-4-R (AGGCCACAACTTTAGCAG)	*Fok*I	322	276, 46

Table S1 continued

Mutant	Alias	Primer name (5' to 3' sequence)	Enzyme	Amplicon size (bp) Wt	Mutant
mdar4-6	R541/ R577	R541-1 (CTGGTGGAGGAAACTGAAGAAAAC) R541-2 (GGACCAAACAACAACAACGATGAT)	*Dde*I	361	181, 180
mdar4-7	R923	R923-JP1 (TGCTGCCAGAAGGTAAG) R923-JP2 (TCAGAAAAGAATCCCGTAG)	*Pst*I	157, 137	294
mfp2-6	R281	MFP2-30 (ATGACATTCTTCCCAGTAGTAAACGAGGCG) MFP2-31 (GATCCCCTCTCAGCCAAAAAAGC)	*Mbo*II	292, 44	227, 64, 44
mfp2-7	R778	R778-1 (AAGTAGCGGCATGATATGAG) R778-2 (CTCAGGATCGAATTGTTGGAGC)	*Alu*I	148, 20	168
mfp2-8	R794/ R809	R794-JP1 (TCTGGCTTTTTCTTTTTCTTTAC) R794-JP2 (TGCCAATTCCAGCCTCCAG)	*Bsm*AI	242	131, 111
mfp2-9	R1009	R794-JP1 (TCTGGCTTTTTCTTTTTCTTTAC) R1009-1 (CAGGAATTTCTCATTTACCG)	*Aci*I	141, 65, 33	141, 85
mls-3	SALK_ 002289	mls-3-1 (AATTTTGTGTTGGGGTTTGAA) mls-3-2 (AGGGTCTCGATAAGCACAGTTG)	-	520	-
		mls-3-1 (AATTTTGTGTTGGGGTTTGAA) LB1-SALK (CAAACCAGCGTGGACCGCTTGCTGCAACTC)	-	-	~280
mls-4	R332	R332-MLS-F (TTGTTCGGTGGTATGATGATCG) R332-MLS-R (ATGCAGATTGGGATGAGTC)	*Taq*I	163	143, 20
ped1-96		PED196-1 (CAATGGCATGGGAAGGGTCAGTCAA) PED196-RsaI (CCCATAGGAAGAAGACAATTGT)	*Rsa*I	156	130, 26
ped1-4	R814	R814-1 (TGAGGGTCTGTCGCTATCTTTTCT) R814-2 (AGTTCTGACAGCCACGGTTTCT)	*Hin*fI	218, 105	163, 105, 55
ped1-5	R883	R123-PED1-F (GCTGCGTTCTATGCTGGTTTC) R123-PED1-R (GCTGCGTTCTATGCTGGTTTC)	*Alu*I	265, 90	157, 108, 90
pmdh1-2	R92	PMDH1-7 (TGTTTTAGGTTCGTGGATTTCTC) PMDH1-2 (ATCATCCCTCGTCATCCCTGGTTTCCTC)	*Aci*I	86, 30	116
pme31-1	R79	R79-PME31-1 (TTATAATTGTCGATTTCTCA) R79-M14-R (GTATCCTGCATTTCACATTTTG)	*Dde*I	158, 17	175
pme31-2	R363	pme31-1-1 (GGCAACGACTCGAATGGTTAGGG) pme31-1-2 (TTCTCAAAAGTAATGTTCTCTGC)	*Hin*fI	141, 99, 84, 74, 9	215, 99, 84, 9
pme31-3	R922	R922-1 (CTGTTACATCGAGGGAAGTGTGG) R922-2 (CGTTTCCCCAGTTATGCCAACCC)	*Bsr*I	219, 6	219, 133, 6
pxa1-1		T5J17-24 (ATGGGAGTCACTTTCATAACCTCATCTCAA) T5J17-25 (CCATCAATCAGCCTTAGCTCCAAGGAATGG)	*Sml*I	150, 30	180
pxa1-4	R751	R751-1 (GCTGGGACGGCGATAAGAAA) R751-2 (GCAACTGTGGCCCCAAGATACT)	*Mnl*I	269	143, 126
pxn-3	SAIL_ 636F12	PXN-1 (CTAATGCAGAAGCTCTGGTTGCTGT) PXN-2 (ATTGCATTGACGGATTACTTAC)	-	~400	-
		LB1-SAIL (GCCTTTTCAGAAATGGATAAATAGCCTTGCTTCC) PXN-1 (CTAATGCAGAAGCTCTGGTTGCTGT)	-	-	~400
pxn-4	R109	R109-1 (CGGAGCTGTGGCGAAACTCGG) R109-AvaII (AATCATTTTCAGAATCGCGTCCAATGGTC)	*Ava*II	196, 29	225
pxn-5	R162	R109-1 (CGGAGCTGTGGCGAAACTCGG) PMP38-1 (GCCCCCGAGTCACCTTCTTC)	*Nru*I	152, 61	213
pxn-6	R986	R986-1 (CCCCGAGTCACCTTCTTCTAATG) R986-2 (AGGCACGCTTTTTCTTCAG)	*Apo*I	449	235, 214
pxn-7	R987/ 995	R995-F (GCTACAGTCACAACTTACCC) R995-HindIII-R (TTCATGATAAGAGGGAAAGC)	*Hin*dIII	111	90, 21
sdp1-6	R330	R330-SDP1-F1 (TAATGACACAAGGGGCTCTACACG) R330-SDP1-R1 (TCACTGCGCTCCATATAACCACAT)	*Sty*I	201	147, 54

Table S2: PCR-based markers used for recombination mapping

Marker	Nearest gene	Primer name (5' to 3' sequence)	Enzyme	Amplicon size (bp) Col	Amplicon size (bp) L*er*
Chromosome 2					
RGA1	*At2g01570*	RGA1-1 (GGTTCGTCCGGTTTAGCGCCGGCAC) RGA1-2 (CAGTTCGGTTTAGGTCTTGGTCCG	*Rsa*I	185, 112	297
T8K22	*At2g02670*	T8K22-1 (TCCGCGAACGAACAGGAG) T8K22-2 (GCAAGGTTTGTGCTAATAA)		123	112
T20F6	*At2g02800*	T20F6-1 (TTCGTGTAGGAGCAATAG) T20F6-2 (CCCTTCGTTCTCAACATC)		168	119
PLS2	*At2g19290*	PLS2-1 (TACGCGAATTATTTTTAGGAGA) PLS2-2 (AATTTATTTTGAGTCGGATGC)		70	80
PedI	*At2g33150*	Ped1-1 (CCAGCCAAGTAAGTGATGGTGCAGG) Ped1-2 (GCAGGGTCAACACCAACTGCAGC)		289	257
SEC 221	*At2g45540*	SEC221-1 (GGTGTTTTTGCATGGTTCTTTCGCTTC) SEC221-TaqI (ATATGAATTTGAACCGCACAATAGCCGTCG)	*Taq*I	172	143, 29
SNP9553	*At2g46720*	SNP9553-1 (TGCGTTTGATGTTTTGAATATGTATGAGAAG) SNP9553-2 (ATATAAAGTCACAATTATTTCGCAGCCG)	*Mbo*II	219	187, 32
Chromosome 3					
nga172	*At3g03340*	nga6172-1 (TACATCCGAATGCCATTGTTCCTATCATTG) nga6172-2 (AGCACATCAAGCTGCTTCCTTATAGCGTCC)		170	150
SEC305	*At3g05850*	SEC305-1 (ATATAGCAAGGCGTGGACAGCAGAG) SEC305-2 (GGGGACCTTATTAGCTGCGACTTCTG)	*Taq*I	73, 71	144
SEC310	*At3g06010*	SEC310-1 (TTGCACTGGTATGAATGTTATGTCTGAAA) SEC310-RsaI (TGCTTTCCTTTCCTCTAAACGTCCATCGTA)	*Rsa*I	75, 25	100
SEC327	*At3g06470*	SEC327-TaqI (CTCTGGGACCCACTTTCATGAAAATTAGTC) SEC327-2 (CGAAGTTTGGGGAGTTGACGTTTGAAGAT)	*Taq*I	100	71, 29
SEC328	*At3g07530*	SEC328-DdeI (AAGCATTGACTCACCAGAGCTATTAGTGTC) SEC328-2 (CTCAAAACAATACTCACAGAATACAATG)	*Dde*I	178	152, 26
SEC320	*At3g07770*	SEC320-1 (AACTAACACGAAAATAAACCAACATACAAAC) SEC320-EcoRI (ACGTTTGATGGTACAATTCATCATGCGAAT)	*Eco*RI	204, 28	232
SEC321	*At3g07810*	SEC321-1 (AAAAACAATAAAGATGCAGAATGGCTACT) SEC321-RsaI (TTTGATTATCCTCGTCTTCTTTCTGGAATG)	*Rsa*I	137, 29	166
SEC316	*At3g08910*	SEC316-1 (GATATCTTCTCGGAGTTCTTTGGCTTC) SEC316-HinfI (AGGGGCAGCTTTCCTCGGTGGAACAAGATT)	*Hin*fI	86	59, 27
SEC314	*At3g10200*	SEC314-1 (CAGGTTGGGGAATATGATGACTAATG) SEC314-MseI (GTTTTCATGACCATCTTTGGGAGCAAATTA)	*Mse*I	132, 28	160
nga162	*At3g13960*	nga6162-F (CATGCAATTTGCATCTGAGG) nga6162-R (CTCTGTCACTCTTTTCCTCTGG)		107	89
MRC8	*At3g18160*	MRC8-F1 (CTCTTTTATACGCAAATATGCCTCAGTAGC) MRC8-R1 (ACTGAAAGATATGTAATACACGGTGTCCT)	*Taq*I	150, 100	250
LCS341	*At3g23633*	LCS341-1 (AGTTTTTCTTCTTTTTGTATTTATGTG) LCS341-HinfI (TTGTGCTTTTGCTTTTTAAAGCCGATT)	*Hin*fI	142, 30	172
LCS336	*At3g25200*	LCS336-1 (AGGTCTGAAAAAGCTGAGTTGAGGTC) LCS336-ScaI (GGAGTCGGATATAGCAGTACCAATACAGTA)	*Sca*I	128, 30	158
F13I12	*At3g47200*	F13I12-F (GATGAACACCAATTCCTCTATGAAGTAAGC) F13I12-R (ATATTTCCTTTCCCGTTAGGTGGTTGTC)	*Rsa*I	180, 63	301
T4C21	*At3g60770*	T4C21-1 (CTTGCTTCCAGTAACACTTTTCACCTGTGG) T4C21-4 (GATGTGTTTGCTTGCACTCTCCAAGTTAGC)	*Apo*I	122, 95	217
Nga6	*At3g62220*	nga66-1 (GTCCAGGGAACTAAAGTGGGTCCCTTGG) nga66-2 (GTCACACCCACAACTCGTAAAGCGCG)		280	250

Table S2 continued

Marker	Nearest gene	Primer name (5' to 3' sequence)	Enzyme	Amplicon size (bp) Col	Amplicon size (bp) L*er*
Chromosome 4					
LCS413	*At4g25150*	LCS413-1 (GGGTTCTTATAATCCACTTCCTC) LCS413-XhoI (GAATCAAGGAGAAGAGAATGAGATTCTCGA)	*Xho*I	163, 30	193
LCS414	*At4g27830*	LCS414-1 (TTTTTGGTTTACATCGCTAC) LCS414-EcoRI (TATTTACACTTCATATTTAAAAATTGAATT)	*Eco*RI	225	195, 30
LW 147	*At4g34270*	Nga1107-1 (GAAGAAATAATTTACTCAAAAGCGCG) Nga1107-2 (GAGCGACGAATCGACAGAATTAGGG)		170	160
Nga1107	*At4g38760*	LW147-1 (TCGAAGGAAACCCAAAAA) LW147-2 (TTGAGGCGTTGAAGGAAG)	*Rsa*I	357, 104	461
LCS416	*At4g39300*	LCS416-1 (ATACTGATTAGATGTGAAACTGGATG) LCS416-XbaI (AATCTAAGACCAACTAGACATATATCTCTA)	*Xba*I	194	163, 31
LCS417	*At4g39350*	LCS417-1 (TATCCCAATCTAATCTATCACAAACCCTTCC) LCS417-2 (AGCCAGCAATGAGCCGACCACCAG)	*Spe*I	279, 156	435
Chromosome 5					
CIW18	*At5g05170*	CIW18-1 (AACACAACATGGTTTCAGT) CIW18-2 (GCCGTTTGTCTCTTCAC)		135	129
nga249	*At5g08550*	nga249-F (TTACCGTCAATTTCATCGCCG) nga249-R (TGGATCCCTAACTGTAAAATCCC)		125	115
nga106	*At5g16520*	nga106-F (GTTATGGAGTTTCTAGGGCACG) nga106-R (TGCCCCATTTTGTTCTTCTC)		150	120
F7K24	*At5g19270*	F7K24-1 (TGCAAAATTCTAGCTATCG) F7K24-2 (ACTTTTGTATGGCTAATGAG)		125	141
MWD9	*At5g22420*	MWD9-1 (TAGGGTCGTGGTTGGTTG) MWD9-2 (CTGGCCTCTCTATCTGATAC)		133	118
GA3	*At5g25900*	GA3-1 (CGGAGGCTATCATGTCCCTGC) GA3-2 (CCCAACGCTTCTTATCCATGTTGC)		156	144
S0191	*At5g37780*	SO191-F2 (AGCATATCTCCACCAATCATGCAAATG) SO191-R2 (GTGAGGCTGATGTTGATGGAGATGGTC)		180	200
K16E1	*At5g42590*	K16E1-F (GGTGTATCGTCATGTGTCTC) K16E1-R (AACTACTAGTTCATTGTAAA)		166	148
MNJ7	*At5g47445*	MNJ7-1 (CGAAGAAGAAGAACTTTCTG) MNJ7-2 (GTTAAGTGTAAACCGGTATG)		111	101
JV57	*At5g60710*	JV57-1 (TCCGATTGGTCTAAAGTACGAC) JV57-2 (TTTGATGGACTCTTACATTGGAAA)		180	140
MBK5	*At5g63640*	MBK5-1 (GTACAAAATCACTGTTGTTTACC) MBK5-2 (CAGCTTGAGCATTTCACAGAGACG)		220	200
MHJ24	*At5g64060*	MHJ24-1 (CACAAGTTCAACATCAGTCGGATG) MHJ24-2 (GTGGAGATTATCTATCTGCTTACC)	*Bsm*AI	300, 150	450
MNA5	*At5g65290*	MNA5-4 (GTTAGAGGCAACGAGATCAGATAG) MNA5-5 (CCGAACCGAGATCGAACCAAGG)	*Msp*A1I	135, 110	245
DDM1	*At5g66750*	DDM1-3 (GGAGCTCGTCGTCTCCGGTTGC) DDM1-4 (CACCGACTCAGCACTAGTCTCCC)	*Rsa*I	470	350, 120
M555	*At5g67620*	M555a-1 (CTCTTGAATTATTAAGTTGACTAG) M555a-2 (CCTTTAATTAGTTATCAAATC)	*Acc*I	155	100, 50

Table S3: Primers used to amplify and sequence candidate genes

Gene	Accession number	Primer A name (5' to 3' sequence)	Primer B name (5' to 3' sequence)
ACX2	*At5g65110*	ACX2-3 (AAGCCCAAAAGCCCACATTACC)	ACX2-4 (GCGTGAACACCCATATCCGAGAC)
		ACX2-5 (TAAGATGGGCGTTCAATACAGG)	ACX2-6 (ACATAAGATTTGAGCCCAGCAGAG)
		ACX2-7 (TCGGTGAGCTTGTAGGTGGTC)	ACX2-8 (GTCCGGGCAGCTGAAGAAAGT)
		ACX2-9 (TGCTTTCCGGGTGAGTTAGTGTTTGC)	ACX2-10 (GGTTATATCGTCGTGCCAGTTC)
CHY1	*At5g65940*	K14B20-1 (CAACTTCCTAAACTAAGCGGGTGAAG)	K14B20-8 (CGAAATCGACCATGGACGGATACACC)
		K14B20-2 (GTCTTACGAAATAGACGCACGC)	K14B20-7 (GCAGCTGAATGCTCTGTCCTTCCAC)
		CHY1-A1 (GGTTTTTGCCATGCCTGAGAC)	CHY1-A2 (CCTGCAATCGCCCTTCCCTTATC)
		CHY1-A3 (TTGCGCAGGTTAGATGTTATTG)	CHY1-A4 (ATTCTGCTCTGCTGCTTTGGTGTC)
DRP3A	*At4g33650*	DRP3A-1 (GCTAAGCACGAAAATCCCGAG)	DRP3A-2 (GATGCAGACGCCACAAAAAGTAG)
		DRP3A-3 (CCCTGTCTTTCATGTGATTTAC)	DRP3A-4 (TGGCCAACAACCTTTCCCTAC)
		DRP3A-5 (TTTTACTGCTCAATTTGCCATC)	DRP3A-6 (AGTCCGAATATCATCATCTGTCAAG)
		DRP3A-7 (CCATGCGAGGACTTGACAG)	DRP3A-8 (CTCGGAAAATTGAAGGGATACC)
		DRP3A-9 (GTAATTTTCTCACCGCTGTC)	DRP3A-10 (AACTGCTATCTCATCTGGCTCTTG)
		DRP3A-11 (AGCCGTTTGTCCATCTTG)	DRP3A-12 (GAATACCGCTGTCCATAACTAAC)
LON2	*At3g06810*	LON2-1s (CTCATAAGTGTTGCCTTTCGCTAAATCCC)	LON2-2s (CCACATTCACTTTCCTGCTGG)
		LON2-3s (CTTATCTTTGATGCCACCAACAGGCAGAAC)	LON2-4s (GTCTGTATTGACTGTTACCCTTAACGG)
		LON2-5s (CAGATGGCGCATAGCTATCTTAAG)	LON2-6s (GATGGTGTGTGACTGTGGACCAACTTG)
		LON2-7s (GGCTAAACCATAGTGATCACTGTCAAGACG)	LON2-8s (TAGTTTCGACTTAGAGCTTATTTGG)
		LON2-9s (CTGGATCTTGTTTTACTTGCTCCAACTC)	LON2-10s (GAAACAGTGGAGCTCCCGAGTAGGTTAGCG)
		LON2-11s (GATCGAAGCGTAAGAATGTTAGGAATTGAG)	LON2-12s (GTAATGTAATGGGCCTTAGTCTCATTGTTTC)
MDAR4	*At3g27820*	MDAR4-1 (ATGATGGGCCAAGCAAGTCGTG)	MDAR4-2 (CCATACCCGGGCACCTGTTG)
		MDAR4-3 (CACGGCTTCCTTCTTTCCACAC)	MDAR4-4 (ATCCCGATACCAACCACAACC)
		MDAR4-5 (AAGGAACGGTTTTGACATC)	MDAR4-6 (TTGCCGAATTAACTCTACC)
MFP2	*At3g06860*	MFP2-20 (AGTACCGTTGCTTTGAGGAGTGTGC)	MFP2-21 (AACATACCATTCCCCTTCTGCATTTCACC)
		MFP2-22 (TGATCTGGTAATGGCTTTTGTGTTCCTTTTT)	MFP2-23 (CCCATGGTTTTCTCCTCCCGACTAT)
		MFP2-24 (GATTTTGGTATGTCAGTGCCTTATTCTTA)	MFP2-25 (CACTTCAGCTTGTTATGTTCATCCTTACC)
		MFP2-26 (TGGAATTGGCAGAGTTAAAGGTGAGG)	MFP2-27 (TGCAATCGCCACACCAAATCCAACC)
		MFP2-28 (ATCCATATCTAATCGACAGGGCAATCAG)	MFP2-29 (TGACAAAGCACAACATAAAACAAATCT)
PED1	*At2g33150*	PED1-20 (AAGCAAAGAAATATTACGAAAAA)	PED1-21 (ATCCCCAGACTGCAAACACAAGAG)
		PED1-16 (ATCTGGGCTTCAGGCTGTTGCTGAT)	PED1-17 (TGCCTTTCTGTGCGAGTCAACCTA)
		PED1-13 (GACATAGGCATTGATAGAGAAGACGAATCT)	PED1-8 (AAGTACCAGCAGTAGTGGTGCCAT)
		PED1-14 (TGTTGACCCGAAGACTGGTGATGAGAAAC)	PED1-15 (AGATATATCTCGGCTGTGGATTTCTTAAGG)
		PED1-11 (GAATCCTTGTGTGTTCAGGCAT)	PED1-12 (AGAAATGGCTGCCACCCAAA)

Table S4: Accession numbers of proteins used for alignments using ClustalW on Lasergene MegAlign (DNAStar)

Organism	Protein abbreviation	Accession number
DRP3A alignment (**Figure 3**)		
Arabidopsis thaliana	DRP3A	At4g33650
Arabidopsis thaliana	DRP1A	NP_851120.1
Oryza sativa		NP_001045220.1
Chlamydomonas reinhardtii		XP_001697229.1
Homo sapiens		NP_056384.2
Dictyostelium discoideum		XP_642112.1
SDP1 alignment (**Figure 5**)		
Arabidopsis thaliana	SDP1	At5g04040
Arabidopsis thaliana	SDP1L	At3g57140
Glycine max		XP_003554141.1
Oryza sativa		NP_001044325.1
Selaginella moellendorffii		XP_002982599.1
Saccharomyces cerevisiae	Tgl4p	NP_013015.1
MDAR4 alignment (**Figure 5**)		
Arabidopsis thaliana	MDAR4	At3g27820
Populus trichocarpa		XP_002298535.1
Glycine max		XP_003553831.1
Oryza sativa		NP_001047875.1
Selaginella moellendorffii		XP_002990620.1
PXA1 alignment (**Figure 6**)		
Arabidopsis thaliana	PXA1	At4g39850
Glycine max		XP_006591509.1
Oryza sativa		NP_001054425.1
Selaginella moellendorffii		XP_002965745.1
Homo sapiens	ABCD1	NP_000024.2
Saccharomyces cerevisiae	Pxa1p	NP_015178.1
ACX1 alignment (**Figure 6**)		
Arabidopsis thaliana	ACX1	At4g16760
Solanum lycopersicum		NP_001234198.1
Oryza sativa		NP_001056542.1
Selaginella moellendorffii		XP_002963293.1
Homo sapiens		NP_004026.2
Saccharomyces cerevisiae		NP_011310.1
ACX2 alignment (**Figure 6**)		
Arabidopsis thaliana	ACX2	At5g65110
Oryza sativa		ABA94669.2
Homo sapiens		NP_003492.2
Saccharomyces cerevisiae		NP_011310.1
MFP2 alignment (**Figure 7**)		
Arabidopsis thaliana	MFP2	At3g06860
Arabidopsis thaliana	AIM1	At4g29010
Solanum lycopersicum		XP_004252912.1
Oryza sativa		NP_001042973.1
Selaginella moellendorffii		XP_002978003.1
Chlamydomonas reinhardtii		XP_001699366.1
Rattus norvegicus		NP_598290.1
Mycobacterium tuberculosis		WP_003404426.1

Table S4 continued

Organism	Protein abbreviation	Accession number
PED1 alignment (**Figure 7**)		
Arabidopsis thaliana	PED1	At2g33150
Helianthus annuus		AAQ77242.1
Oryza sativa		NP_001048523.1
Selaginella moellendorffii		XP_002963753.1
Homo sapiens	ACAA1	NP_001598.1
Saccharomyces cerevisiae	Pot1p	NP_012106.1
Thermus thermophilus		WP_011228352.1
CHY1 alignment (**Figure 7**)		
Arabidopsis thaliana	CHY1	At5g65940
Oryza sativa		NP_001066529.1
Selaginella moellendorffii		XP_002982321.1
Homo sapiens		NP_055177.2
Saccharomyces cerevisiae	Ehd3p	NP_010321.1
Mycobacterium thermoresistibile		WP_003924040.1
ICL alignment (**Figure 8**)		
Arabidopsis thaliana	ICL	At3g21720
Glycine max		NP_001239869.1
Oryza sativa		NP_001059839.1
Selaginella moellendorffii		XP_002981082.1
Saccharomyces cerevisiae	Icl1p	NP_010987.3
LON2 alignment (**Figure 12**)		
Arabidopsis thaliana	LON2	At5g47040
Glycine max		XP_003549964.1
Oryza sativa		NP_001063769.1
Selaginella moellendorffii		XP_002974838.1
Homo sapiens	LON2	NP_113678.2
Saccharomyces cerevisiae	Pim1p	NP_009531.1
Bacillus subtilis		WP_038827668.1
PME31 alignment (**Figure 15**)		
Arabidopsis thaliana	PME31	At3g29090
Arabidopsis thaliana	PME2	At1g53830
Arabidopsis thaliana	PME53	At5g19730
Solanum lycopersicum	PME31	XP_004253337.1
Solanum lycopersicum	PME1	P14280.5
Zea mays		XP_008661243.1
Dickeya dadantii	PME	1QJV_A

Table S5: Summary of whole-genome sequencing strategies and results

Mutant	Allele	Lines sequenced	Number of homozygous EMS[1] mutations in exons and splice sites
R330	*sdp1-6*	7 pooled F_3 lines	6
R751	*pxa1-4*	5 pooled M_4 lines	74
R574	*acx1-4*	11 pooled F_3 lines	7
R778	*mfp2-7*	5 pooled F_3 lines	6
R809	*mfp2-8*	6 pooled F_3 lines	15
R332	*mls-4*	14 pooled F_3 lines	5
R291	*icl-3*	7 pooled F_3 lines	6
R601	*icl-4*	14 pooled F_3 lines	2
R951	*icl-5*	7 pooled M_4 lines	34
R92	*pmdh1-2*	10 pooled F_3 lines	15
R541	*mdar4-6*	19 pooled F_3 lines	1
R577	*mdar4-6*	3 pooled M_4 lines	54
R109	*lon2-8*	5 pooled F_3 lines	21
R402	*drp3a-5*	42 pooled F_3 lines	5
R79	*pme31-1*	11 pooled F_3 lines	4
R363	*pme31-2*	18 pooled F_3 lines	7
R992	*pme31-3*	4 pooled M_4 lines	58

[1]EMS mutations include those consistent with EMS mutagenesis: G-to-A or C-to-T

Table S6: PCR-based genotyping markers used for recombination mapping in the backcross for R79 (*pme31-1*) and R363 (*pme31-2*)

Mutated gene	Primer name (5' to 3' sequence)	Enzyme	Amplicon size (bp)	
			Wt	Mutant
	R79 (*pme31-1*)			
At3g01085	R79-M1-F (TCCGGAGAAAAGATTATG)			
	R79-M1-R (GAAGAACAACAACAAACCACAGAG)	*Apo*I	274, 61, 42	193, 81, 61, 42
At3g07750	R79-M3-F (GGTGTTATTCCGCAGGTAGTG)			
	R79-M3-R (ATAGAACGATAGAACGGGTGTGAC)	*Bsa*XI	285, 131	416
At3g17750	R79-M5-F (TTGGGAAGAAAAACACGAG)			
	R79-M5-R (CGCCAAAGCCAAAAATCAAG)	*Mnl*I	280, 75	355
At3g22100	R79-M13-F (CCAACGGAGTGAAGCAATCTGAG)			
	R79-M13-R (GACACCACCACCACCACCACAC)	*Bcc*I	242, 41, 59	283, 59
At3g23110	R79-M12-F (CAGTCCAGTTGGCAAAATAGTCTT)			
	R79-M12-R (TGCGAAACAACAGTCTAAGTGGA)	*Ava*II	240, 111	341
At3g24550	R79-PERK1-F (GGCCGGTGTTCAAAGATTAC)			
	R79-PERK1-R (ACCTCAGTGACAAACAAAGACAG)	*Bsm*AI	318	162, 156
At3g27480	R79-M11-F (AAAGCTGCACCTATCAAAATATGAAG)			
	R79-M11-R (ATCTGCCCCATTCCATCTG)	*Ava*II	56, 26	83
At3g52550	R79-M7-F (TGGGTCCGCATCAATCAT)			
	R79-M7-R (ATCCACCATCGACACCATAGAA	*Aci*I	213, 155, 6	368, 6
At3g58790	R79-M8-F (GGCTTCATCACTCAGTTTTCTCTT)			
	R79-M8-R (AGGGGCTTTACCACCGACATT)	*Apo*I	204, 146	146, 113, 91
	R363 (*pme31-2*)			
At3g06810	R363-IBR3-1 (TAAAGGAAATGGCAAAGAGAGAAGGCCCAT)			
	R363-IBR3-2 (CGGTAGCCGCCAGTTCTCTTCTAGC)	*Nco*I	140, 30	170
At3g24780	At3g24780-1 (ACCCCTGCCTCGACTTCTTCTTTC)			
	At3g24780-2 (GACCCCTACTACGACCACCACCAA)	*Nco*I	223, 185	408
At3g29070	At3g29070-1 (AGAGGTGGAGGTGAGGAAACTACT)			
	At3g29070-2 (AACGGTCCAAAATACAGAGAACAA)	*Dde*I	278, 108, 89	386, 89
At3g46530	At3g46530-1 (ATGGTATAGGAGGCTTGAA)			
	At3g46530-2 (TTTAATACGCGTAGTGATGA)	*Xmn*I	199, 198, 142	341, 189

Table S7: Summary of mutant phenotypes

Gene	Allele	Sucrose dependence	IBA or 2,4-DB response	Peroxisome distribution	Peroxisome size	PTS2 processing	PTS1 import
SDP1	*sdp1-7*	Wt	Wt	Clustered	Wt	ND	Wt
PXA1	*pxa1-4*	Dependent	Resistant	Clustered	Wt	Wt	Wt
ACX1	*acx1-4*	Wt	Resistant	Clustered	Large	Wt	Wt
ACX2	*acx2-2*	Wt	Wt	Clustered	Large	Wt	Wt
	acx2-3	Wt	Wt	Clustered	Large	Wt	Wt
MFP2	*mfp2-6*	Partial	Wt	Clustered	Large	Defect	Defect
	mfp2-7	Wt	Slight resistance	Clustered	Large	Wt	Wt
	mfp2-8	Partial	Wt	Clustered	Large	Defect	Defect
	mfp2-9	Partial	Wt	Clustered	Large	Defect	Wt
PED1	*ped1-4*	Dependent	2,4-DB resistant	Clustered	Large	Defect	Defect
	ped1-5	Dependent	Resistant	Clustered	Large	Defect	Defect
MLS	*mls-4*	Partial	Wt	Clustered	Wt	Wt	Wt
ICL	*icl-3*	Wt	Wt	Clustered	Wt	Wt	Wt
	icl-4	Wt	Wt	Clustered	Wt	Wt	Wt
	icl-5	Partial	Wt	Clustered	Wt	Wt	Wt
PMDH1	*pmdh1-2*	Wt	2,4-DB resistant	Clustered	Wt	ND	Wt
CHY1	*chy1-5*	Dependent	Resistant	Clustered	Large	Defect	Defect
	chy1-6	Dependent	Resistant	Clustered	Large	Defect	Defect
	chy1-7	Dependent	Resistant	Clustered	Large	Defect	Defect
MDAR4	*mdar4-5*	Dependent	Wt	Clustered	Wt	ND	Wt
	mdar4-6	Dependent	Wt	Clustered	Wt	ND	Wt
	mdar4-7	Dependent	Wt	Clustered	Wt	ND	Wt
LON2	*lon2-8*	Wt	Resistant (lateral roots)	ND	Large	Defect	Defect
	lon2-9	Wt	Slightly resistant (lateral roots)	ND	Large	Wt	Defect
	lon2-10	Wt	Resistant (lateral roots)	ND	Large	Defect	Defect
PXN	*pxn-4*	Wt	Wt	ND	Large	Wt	Wt
	pxn-5	Wt	Wt	ND	Large	Wt	Wt
	pxn-6	Wt	Wt	ND	Large	Wt	Wt
	pxn-7	Wt	Wt	ND	Large	Wt	Wt
DRP3A	*drp3a-4*	Wt	Wt	Wt	Large	ND	Wt
	drp3a-5	Wt	Wt	Wt	Large	ND	Wt
PME31	*pme31-1*	Wt	Wt	Clustered	Wt	ND	Wt
	pme31-2	Wt	Wt	Clustered	Wt	ND	Wt
	pme31-3	Wt	Wt	Clustered	Wt	ND	Wt

ND, not determined.

File S1 Mutations identified through whole-genome sequencing. (.xlsx, 499 KB)

Available for download as an .xlsx file at
www.genetics.org/lookup/suppl/doi:10.1534/genetics.116.193169/-/DC1/FileS1.xlsx